Computational and Applied Mathematics (2025) 44:148
https://doi.org/10.1007/s40314-025-03107-z

Tracking interfaces in a random logistic free-boundary diffusion problems: a random level set method

Vera Egorova[1] · M. C. Casabán[2] · Rafael Company[2] · Lucas Jódar[2]

Received: 19 June 2024 / Revised: 30 October 2024 / Accepted: 13 January 2025

Abstract

Free-boundary diffusive logistic model finds applications in diverse fields associated with population dynamics. These processes often possess stochastic characteristics and involve parameters with uncertainties. This study focuses on enhancing a two-dimensional diffusive logistic partial differential model with free boundary by incorporating randomness in the mean square sense, considering the conditions for well-posedness in the random case, which is crucial for the further analysis. Both unknown stochastic processes the solution and its moving front, and the parameters involved in the random problem as random variables, are constrained by a finite degree of randomness. To tackle this challenge, we propose a random level set method. Given the complexity of the problem, we employ alternating direction explicit methods for the interior solvers, to effectively address computational challenges. Since computing the mean and the standard deviation of both unknown stochastic processes are required, we combine the sample approach of the difference schemes together with Monte Carlo technique avoiding the storage accumulation of symbolic expressions of all the previous levels of the iteration process. Parallel computing is employed to enhance performance. A careful numerical analysis is performed in the mean square context to ensure stability, positivity, and boundedness. The set of presented examples illustrates these qualitative properties, assess numerical convergence and enables us to gain a deeper understanding of the system's behavior attending to the geometry of the initial habitat. This approach provides valuable tools for analyzing and predicting spreading-vanishing dichotomy.

M. C. Casabán, Rafael Company and Lucas Jódar contributed equally to this work.

✉ Vera Egorova
vera.egorova@unican.es

M. C. Casabán
macabar@imm.upv.es

Rafael Company
rcompany@imm.upv.es

Lucas Jódar
ljodar@imm.upv.es

[1] Depto. de Matemática Aplicada y Ciencias de la Computación, Universidad de Cantabria, Avda. de los Castros, s/n, 39005 Santander, Spain

[2] Instituto Universitario de Matemática Multidisciplinar, Universitat Politècnica de València, Camino de Vera s/n, 46022 Valencia, Spain

Published online: 29 January 2025

Keywords Random Stefan problem · Mean square calculus · Finite degree of randomness · Diffusive logistic model · Level set method · Alternating direction explicit method.

Mathematics Subject Classification 92D25 · 35R35 · 35R60 · 65N06

1 Introduction

The diffusive logistic model finds widespread application in ecological modeling (Malchow 2008), biological invasions (Shigesada and Kawasaki 1997), population dynamics (Aronson and Weinberger 1978), among other fields. Traditionally, analyses in these areas have been framed within a deterministic context. A novel modification of the classical Fisher-KPP diffusive logistic model (Fisher 1937; Kolmogorov et al. 1937) has been introduced in Du and Lin (2010) by incorporating a Stefan-type condition for the boundary, thereby converting the problem into a free boundary problem. This adaptation requires the simultaneous determination of the moving front and the unknown population density, adding a layer of complexity and realism to the model. While the initial focus was on one-dimensional scenarios (Du and Lin 2010), subsequent research expanded this framework to two-dimensional cases with radial symmetry (Du and Guo 2011) and general 2D case (Liu et al. 2020). Despite these advancements, the inherent stochastic characteristics of these processes, including spatial heterogeneity, contact distribution, sexual distribution among the population, the rate of increase of the population, the speed of the wind in a direction, and environmental conditions, necessitate the integration of stochastic elements into the modelling framework.

To analyse systems characterized by intrinsic randomness, Stochastic Partial Differential Equations (SPDEs) can be employed. For instance, Arif et al. (2023), and references therein, present numerical methods for solving stochastic, time-dependent PDEs. In Méndez et al. (2011), the authors investigate the density profiles and invasion front velocities in one-dimensional infinite habitats under environmental fluctuations by transforming a stochastic reaction-diffusion equation into a deterministic equation that incorporates the systematic effects of noise. In Cartwright and Gottwald (2019), the authors employ collective coordinates to simplify infinite-dimensional SPDEs with symmetry into a finite set of Stochastic Differential Equations (SDEs) in application to population dynamics, addressing multiplicative noise and additive symmetry-breaking noise.

An alternative method involves the use of random partial differential equations (RPDEs) through mean square calculus, Soong (1973), which offer flexibility in modeling by allowing the randomization of various model components, including initial/boundary conditions and coefficients. Moreover, this approach permits the assignment of diverse probability distributions to each term of the RPDE, such as exponential, beta or Gaussian distributions, for instance, offering a more nuanced modeling strategy compared to the uniform application of a single stochastic pattern across the entire model, as seen with SPDEs. As highlighted in the literature, parametric RPDEs are increasingly recognized as powerful tools for modeling real-world problems (Kloeden and Han 2017). In particular, the incorporation of randomness into the parameters of diffusive logistic models provides a more accurate representation of phenomena such as population growth and dispersion, more faithfully mirroring the natural variability observed in environmental systems.

PDE problems often involve an additional degree of difficulty: the domain of the solution is itself unknown and must be determined as part of the solution process. These are termed free-boundary PDEs. They play a crucial role in deterministic modeling across diverse fields,

from physics and engineering (Aiki and Muntean 2013; Mitchell and Vynnycky 2016; Nepal et al. 2023; Singla et al. 2024), wildfire propagation (Mentrelli and Pagnini 2016) to finance (Egorova et al. 2017). By incorporating this ingenious concept, free-boundary PDE problems unlock a deeper understanding of how phenomena spread and interact with their environment.

Free boundary PDE problems pose significant computational challenges. Due to this complexity, researchers have focused on developing numerical methods to find approximate solutions, particularly in one or two-dimensional geometries. These methods include the exponential time differencing method (Liu and Liu 2024), the front-tracking method (Nandi and Sanyasiraju 2022), the front-fixing method (Piqueras et al. 2017), the level set method (Khan et al. 2021), among others.

The concept of a free boundary holds particular significance in RPDEs for diffusive logistic models. In this context, the free boundary represents the random spreading front of the population or phenomenon under consideration. This random front is influenced by factors such as population growth, diffusion characteristics, and environmental parameters that may vary randomly. Hence, the free boundary becomes a stochastic process alongside the population density, as has been shown in Casabán et al. (2024).

In this study, we expand our investigation into a random diffusive logistic model, building on the prior work by Casabán et al. (2024), which examined a multidimensional random scenario characterized by radial symmetry. With this assumption, the complex multidimensional problem is reformulated as a one-dimensional random PDE with a moving radius of the boundary. To address this problem in a m.s. sense, we have developed the random front-fixing method and the random front-tracking method for the first time in Casabán et al. (2024), to our knowledge. Now, we're taking a step further by not assuming that everything has to spread out with radial symmetry. This allows us to develop a more detailed model that better captures the dynamics of a spreading or diffusing quantity in a domain with a moving boundary.

Given the high-dimensional nature of these problems, numerical methods play a crucial role in their analysis. These methods provide approximations of the solutions and facilitate the investigation of system behavior under various scenarios. To efficiently and accurately solve the random partial differential equation problem and track the random free boundary, we propose the use of a random explicit Level Set Method (RLSM). This method in the deterministic scenario, developed in Osher and Sethian (1988), has demonstrated a strong ability to accurately capture the initial configuration in free boundary problems, producing stable results even with irregular initial geometries, see for details (Sethian 1996; Gibou et al. 2018). This approach allows for a detailed representation of complex contours at the free boundary and adapts as the domain evolves without introducing significant numerical instabilities. Specifically, LSM is particularly effective in handling problems with nonlinear dynamics and changing boundary shapes, as it can reliably update geometry over time, as demonstrated in prior studies (Osher and Fedkiw 2001; Wei et al. 2020). Therefore, counterpart in the random framework is well-suited for the proposed RPDE model. For the random numerical solution of the underlying RPDE, we propose various random mean square finite difference schemes (RFDS) (Casabán et al. 2021). In our study, instead of using the traditional forward Euler method for the interior solvers, as employed in deterministic cases like those in Liu et al. (2020), or in random cases with radial symmetry such as Casabán et al. (2024), we implemented Alternating Direction Explicit (ADE) methods. This choice enhances stability, particularly when applied in conjunction with the LSM, which excels at capturing complex initial configurations in free boundary problems, even with irregular geometries.

To analyze the resulting RPDE model, we use the Monte Carlo technique, which effectively handles randomness in computational models. Traditional iterative methods, like finite difference schemes, are unsuitable for random scenarios due to excessive storage demands from symbolic computations at intermediate levels (Casabán et al. 2020). To address this, we combine the sample m.s. approach with the Monte Carlo method, achieving efficient computation without overwhelming storage requirements. Through Monte Carlo simulations, we calculate the statistical moments of the pairwise of unknown stochastic processes (s.p.'s), that it, the approximate population density and the moving boundary s.p.'s. This analysis will provide valuable insights into the probabilistic behavior of the system, particularly its impact on the spreading-vanishing dichotomy, which represents a fundamental characteristic of the diffusive logistic model with Stefan-type free boundary condition. Moreover, it is necessary that the reliability of the numerical results is established due to in many cases the exact solution in not available. For this purpose, we will use a Cauchy type condition guarantying the numerical convergence of the Monte Carlo method.

This paper is organized as follows. Section 2 reviews key definitions related to mean square and mean four calculus. Section 3 introduces a two-dimensional random logistic diffusion model with a free boundary. Section 4 proposes a RLSM for the model, along with the underlying RFDS. We consider three RFDS, those qualitative properties are analyzed in Sect. 5. Section 6 summarizes the proposed numerical algorithm. Numerical examples and simulations are presented in Sect. 7 to validate and demonstrate the effectiveness of our approach. We examine the qualitative properties of the proposed random finite difference schemes, such as stability and convergence of the numerical solutions, and showcase the practical application of our enhanced model in various habitat shapes. These examples provide valuable insights into the behavior of the system under stochastic conditions, offering a deeper understanding of the dynamics and facilitating decision-making in real-world applications. A set of conclusions are given in Sect. 8.

2 Some preliminaries on the mean square (m.s.) and mean four (m.f.) calculus

In this work the mathematical treatment of randomness in RPDE will be performed using the so-called $L_p(\Omega)$ calculus providing a handle rigorously uncertainty in those equations. Concretely, we are interested in $L_2(\Omega)$ and $L_4(\Omega)$ calculus which are usually referred to as mean square (m.s.) and mean four (m.f.) calculus, see Soong (1973) and Villafuerte et al. (2010). We note that the m.s. approach has the property that the m.s. solution coincides with the one obtained in the deterministic case, that is, when the random data become deterministic. Although the m.s. calculus is developed in the $L_2(\Omega)$ space it requires of the spaces $L_p(\Omega)$, $p > 2$, to establish some results, such us the m.s. convergence (Soong 1973). These spaces verify that $L_q(\Omega) \subset L_p(\Omega)$, for $q > p$. In the context of this paper we will construct the solution s.p.'s in the particular cases $p = 2$ and $p = 4$. The $L_p(\Omega)$ spaces are made by all real-valued r.v.'s, $X(\omega)$, defined on a probabilistic space $(\Omega, \mathcal{F}, \mathbb{P})$ satisfying that statistical moments of order p are finite, that it, $\mathbb{E}\left[|X(\omega)|^p\right] < +\infty$, where $\mathbb{E}[\cdot]$ denotes the expectation operator. Many probability distributions such as binomial, Poisson, beta, exponential or Gaussian have statistical moments of any order, then they belong to $L_p(\Omega)$, $p > 2$, and therefore also to $L_2(\Omega)$. For short, in the sequel these r.v.'s will be referred to as p-r.v.'s. The space $L_p(\Omega)$ endowed with the following norm, $\left(L_p(\Omega), \|\cdot\|_p\right)$, is a Banach

space (Soong 1973, p. 9)

$$\|X(\omega)\|_p = \left(\mathbb{E}\left[|X(\omega)|^p\right]\right)^{1/p} = \left(\int_\Omega |X(\omega)|^p f_{X(\omega)}\, \mathrm{d}\omega\right)^{1/p} < +\infty, \tag{1}$$

where $f_{X(\omega)}$ denotes the density function of the r.v. $X(\omega)$ and $\omega \in \Omega$ an event of the sample space Ω. There are difficulties with the m.s. operational calculus due to the fact that the $\|\cdot\|_p$ is not sub multiplicative, that is, it does not satisfy the Banach inequality. But, using Schwarz inequality (Soong 1973, p. 43), one obtains the following inequality $\|X(\omega)\,Y(\omega)\|_p \le \|X(\omega)\|_{2p}\,\|Y(\omega)\|_{2p}$, that is, for $p = 2$ one gets

$$\|X(\omega)\,Y(\omega)\|_2 \le \|X(\omega)\|_4\,\|Y(\omega)\|_4, \quad \forall X(\omega), Y(\omega) \in L_4(\Omega),$$

which permits to establish that m.f. convergence entails m.s. convergence by specializing it for $Y(\omega) = 1$. Then a m.f. calculus is necessary to get the m.s. results for solving linear RPDE in the m.s. sense. The role of functions are played by stochastic processes (s.p.'s), which are defined by a sub-sequence of t-indexed r.v.'s $\{X(t;\omega) : t \in T \subset \mathbb{R}\}$ of order p, called p-s.p.'s, verifying $\mathbb{E}\left[|X(t;\omega)|^p\right] < +\infty$, $\forall t \in T$. We recall that q-convergence entails p-convergence, whenever $q > p$. A p-s.p. $X(t;\omega)$ is called p-continuous at $t \in T$ if

$$\|X(t+\delta;\omega) - X(t;\omega)\|_p \to 0 \quad \text{as } \delta \to 0,\ t, t+\delta \in T,\ \forall \omega \in \Omega.$$

A p-s.p. is called p-differentiable at $t \in T$ if there exists the p-derivative of $X(t;\omega)$, namely $X'(t;\omega)$, verifying

$$\left\| \frac{X(t+\delta;\omega) - X(t;\omega)}{\delta} - X'(t;\omega) \right\|_p \to 0 \quad \text{as } \delta \to 0,\ t, t+\delta \in T,\ \forall \omega \in \Omega.$$

3 A 2D-random logistic diffusion model

We consider a random two-dimensional (2D) logistic diffusion model in the m.s. sense where the random population density of a spreading species, depending on time t and spatial variables $(x, y) = \mathbf{x}$, will be denoted by $u(\mathbf{x}, t;\omega)$ and the population's habitat (domain) by $\Phi(t;\omega)$. This model is characterized by a set of equations that dictate the evolution of $u(\mathbf{x}, t;\omega)$ over time and across space in the m.s. sense as follows

$$\begin{aligned} &u_t(\mathbf{x}, t;\omega) - D(\omega)\,\Delta u(\mathbf{x}, t;\omega) = u(\mathbf{x}, t;\omega)\,(\alpha(\mathbf{x}) - \beta(\mathbf{x})\,u(\mathbf{x}, t;\omega))\,, \\ &\quad t > 0,\ \mathbf{x} \in \Phi(t;\omega),\ \omega \in \Omega, \end{aligned} \tag{2}$$

subject to the boundary and initial conditions, respectively,

$$u(\mathbf{x}, t;\omega) = 0,\ t > 0, \quad \mathbf{x} \in \partial\,\Phi(t;\omega),\ \omega \in \Omega, \tag{3}$$

$$u(\mathbf{x}, 0;\omega) = u_0(\mathbf{x}), \quad \mathbf{x} \in \Phi(0;\omega) = \Phi_0,\ \omega \in \Omega, \tag{4}$$

and the random Stefan condition

$$v(\mathbf{x}, t;\omega) = -\eta(\omega)\,\nabla u(\mathbf{x}, t;\omega),\ t > 0, \quad \mathbf{x} \in \partial\,\Phi(t;\omega),\ \omega \in \Omega. \tag{5}$$

Here, the couple of unknowns $(u(\mathbf{x}, t;\omega), \partial\Phi(t;\omega))$ are 4-s.p.'s, with additional conditions to be specified later, defined in a complete probability space $(\Omega, \mathcal{F}, \mathbb{P})$ being ω an event of the sample space Ω and $\partial\,\Phi(t;\omega)$ the edge of the population's habitat $\Phi(t;\omega)$ that changes in time, that is, the random moving boundary or front of the model. In RPDE (2), Laplacian

operator $\triangle\, u(\mathbf{x}, t; \omega) = \frac{\partial^2 u(\mathbf{x},t;\omega)}{\partial x^2} + \frac{\partial^2 u(\mathbf{x},t;\omega)}{\partial y^2}$ indicates spatial diffusion and $D(\omega)$ is a positive random variable (r.v.) which denotes the diffusion coefficient bounded such that

$$0 < d_1 \leq D(\omega) \leq d_2, \quad \forall \omega \in \Omega. \tag{6}$$

The right-hand side of (2) encapsulates a deterministic logistic growth-term, with the positive continuous real functions $\alpha(\mathbf{x})$ and $\beta(\mathbf{x})$ such that

$$\exists\, \kappa_1, \kappa_2 > 0 : \quad \kappa_1 \leq \alpha(\mathbf{x}) \leq \kappa_2, \qquad \kappa_1 \leq \beta(\mathbf{x}) \leq \kappa_2, \quad \forall \mathbf{x} \in \mathbb{R}^2_+. \tag{7}$$

The function $\alpha(\mathbf{x})$ denotes the intrinsic growth rate and the quotient $\frac{\alpha(\mathbf{x})}{\beta(\mathbf{x})}$ is the carrying capacity of the species. The random Stefan's condition (5) describes the random velocity $v(\mathbf{x}, t; \omega)$ of the random moving boundary in relation with the random population gradient at the points of the random moving boundary. The positive r.v. $\eta(\omega)$, denoting the proportionality between the random population gradient at the moving boundary and the velocity of the random moving front, is taking bounded as follows

$$0 < \eta_0 \leq \eta(\omega), \quad \forall \omega \in \Omega. \tag{8}$$

The initial population density function $u_0(\mathbf{x})$ is assumed to have the following properties

$$u_0(\mathbf{x}) \in \mathcal{C}^2\,(\Phi_0); \qquad u_0(\mathbf{x}) > 0, \;\; \forall \mathbf{x} \in \Phi_0; \qquad u_0(\mathbf{x}) = 0, \;\; \forall \mathbf{x} \in \partial\Phi_0. \tag{9}$$

For the sake of practical application, we adopt the useful method of specifying a s.p. in terms of an analytic formula of the real variables $\mathbf{x}$ and t containing r.v.'s as parameters (Soong (1973), p.36–37). In this case the uncertainty into the solution s.p.'s is limited to a finite degree of randomness, i.e. the

unknown s.p.

$u(\mathbf{x}, t; \omega)$

depends on a finite number q of r.v.'s

$$u(\mathbf{x}, t; \omega) = g\left(\mathbf{x}, t; A_1(\omega), \ldots, A_q(\omega)\right). \tag{10}$$

where

$$\left.\begin{array}{r} A_i(\omega),\;\; B_i(\omega), i = 1, \ldots, q, \text{ are mutually independent r.v.'s;} \\ g \text{ is a second order differentiable real function on variable } \mathbf{x}\,; \\ g \text{ is a differentiable real function on variable } \;t. \end{array}\right\} \tag{11}$$

This random framework has been presented in recent works involving random Stefan problems (Casabán et al. 2024), and references therein.

4 A random level set method

The level set method (LSM) is a powerful numerical technique used for tracking evolving interfaces and shapes, see Osher and Fedkiw (2003) and Osher and Sethian (1988). In this section we propose a random level set method (RLSM) to address the study of the random free boundary logistic problem described by (2)–(11). Following the ideas of the LSM, we are going to employ it to track the random boundary of the population's habitat, $\partial\Phi(t; \omega)$, $\omega \in \Omega$, at each new time-step and a random explicit finite difference scheme (RFDS, Casabán et al. 2021) to solve numerically the RPDE (2) everywhere away from the random front.

Initially, level set function $\varphi(\mathbf{x}, 0)$ is defined as the signed distance function

$$\varphi(\mathbf{x}, 0) = \begin{cases} -d, & \mathbf{x} \in \Phi_0, \\ 0, & \mathbf{x} \in \partial\Phi_0, \\ d, & \mathbf{x} \in \mathbb{R}^2 - \Phi_0, \end{cases} \tag{12}$$

where d is the distance from the point $\mathbf{x}$ to the deterministic initial front $\partial\Phi_0$.

For $t > 0$, we construct a level set 4-s.p. $\varphi(\mathbf{x}, t; \omega)$, as analytic formula of the real variables $\mathbf{x}$ and t containing a finite number of r.v.,

$$\varphi(\mathbf{x}, t; \omega) = \tilde{f}\left(\mathbf{x}, t; C_1(\omega), \ldots, C_q(\omega)\right), \tag{13}$$

where $C_i(\omega)$, $i = 1, \ldots, q$, are mutually independent r.v.'s and $\tilde{f}$ is a differentiable real function on variables $\mathbf{x}$ and t.

For each sample realization $\omega_\ell \in \Omega$, $\varphi(\mathbf{x}, t; \omega_\ell)$ is defined by

$$\varphi(\mathbf{x}, t; \omega_\ell) = \begin{cases} -d(\mathbf{x}, t; \omega_\ell), & \mathbf{x} \in \Phi(t; \omega_\ell), \\ 0, & \mathbf{x} \in \partial\Phi(t; \omega_\ell), \\ d(\mathbf{x}, t; \omega_\ell), & \mathbf{x} \in \mathbb{R}^2 - \Phi(t; \omega_\ell), \end{cases} \tag{14}$$

where $d(\mathbf{x}, t; \omega_\ell) = \min_{\mathbf{z} \in \partial\Phi(t;\omega_\ell)} \|\mathbf{x} - \mathbf{z}\|$. Then, for any time $t > 0$ and for each event $\omega_\ell \in \Omega$, the expanding front is equal to the zero level set of $\varphi(\mathbf{x}, t; \omega_\ell)$:

$$\partial\Phi(t; \omega_\ell) = \{\mathbf{x} \in \Phi(t; \omega_\ell) \,:\, \varphi(\mathbf{x}, t; \omega_\ell) = 0\}, \ \omega_\ell \in \Omega. \tag{15}$$

The evolution of the interface $\partial\Phi(t; \omega)$ is subsequently computed by solving the following RPDE for the level set s.p., as it is done for the deterministic case in Liu et al. (2020):

$$\varphi_t(\mathbf{x}, t; \omega) + V(\mathbf{x}, t; \omega)\,|\nabla\varphi(\mathbf{x}, t; \omega)| = 0, \quad \omega \in \Omega, \tag{16}$$

where $V(\mathbf{x}, t; \omega)$ is a m.f. continuous extension of 4-s.p. $|v(\mathbf{x}, t; \omega)|$ described by the Stefan's condition (5), from the front $\partial\Phi(t; \omega)$ over the whole computational domain. Hence, the governing RPDE (16) for the level set s.p. can be written as follows,

$$\varphi_t(\mathbf{x}, t; \omega) - \eta(\omega)\nabla u(\mathbf{x}, t; \omega) \cdot \nabla\varphi(\mathbf{x}, t; \omega) = 0, \quad \omega \in \Omega. \tag{17}$$

Following the ideas developed in Casabán et al. (2021), we will construct a random explicit difference scheme for the RPDE (17) to solve it numerically throughout the approximation of their m.s. derivatives by difference approximations. To this end, we discretize the spatial domain considering a rectangular computational domain, denoted as $\Sigma = [x_{\min}, x_{\max}] \times [y_{\min}, y_{\max}]$, such that $\Phi(t; \omega)$ is a subset of Σ for all $t \in [0,\ T]$. The domain is discretized using a uniform grid, defined as follows:

$$x_i = x_{\min} + ih_x, \quad h_x = \frac{x_{\max} - x_{\min}}{N_x}, \quad i = 0, \ldots, N_x, \tag{18}$$

$$y_j = y_{\min} + jh_y, \quad h_y = \frac{y_{\max} - y_{\min}}{N_y}, \quad j = 0, \ldots, N_y. \tag{19}$$

Here, x_i and y_j denote the coordinates in the x and y directions respectively of a given (i, j)-grid point. The grid spacing in the x and y directions are represented by h_x and h_y, respectively. The total number of grid points in the computational domain is consequently $(N_x + 1)(N_y + 1)$. Analogously, the temporal discretization is defined as follows:

$$t^n = nk, \quad k = \frac{T}{N_t}, \quad n = 0, \ldots, N_t. \tag{20}$$

The numerical approximation of the population distribution s.p. at the grid points (x_i, y_j), where $0 \le i \le N_x$ and $0 \le j \le N_y$, at the time level t^n (where $0 \le n \le N_t$) is denoted by $U^n_{i,j}(\omega) \approx u(x_i, y_j, t^n; \omega)$, $\omega \in \Omega$. From the initial condition (4), we can deduce that the initial distribution of the population is given by

$$U^0_{i,j} = u_0(x_i, y_j), \quad 0 \le i \le N_x, \ 0 \le j \le N_y. \tag{21}$$

We denote $\phi^n_{i,j}(\omega) \approx \varphi(x_i, y_j, t^n; \omega)$, $\omega \in \Omega$, as the approximation of the level set s.p. at the grid point (x_i, y_j) at time level t^n. The initial values are computed as follows

$$\phi^0_{i,j} = \begin{cases} -d, & (x_i, y_j) \in \Phi_0, \\ 0, & (x_i, y_j) \in \partial\Phi_0, \\ d, & (x_i, y_j) \in \Sigma \setminus \Phi_0, \end{cases} \tag{22}$$

where d is the distance from the grid point to the front.

In order to construct a RFDS, we approximate the m.s. time derivative using forward time-stepping of the first order:

$$u_t(x_i, y_j, t^n; \omega) = \frac{U^{n+1}_{i,j}(\omega) - U^n_{i,j}(\omega)}{k} + \mathcal{O}(k), \tag{23}$$

$$\varphi_t(x_i, y_j, t^n; \omega) = \frac{\phi^{n+1}_{i,j}(\omega) - \phi^n_{i,j}(\omega)}{k} + \mathcal{O}(k), \tag{24}$$

where $0 \le i \le N_x$, $0 \le j \le N_y$, $\omega \in \Omega$, and we use central finite difference approximations of the second order for the m.s. spatial derivatives in the interior nodes of the computational domain, where $1 \le i \le N_x - 1$, $1 \le j \le N_y - 1$ and $\omega \in \Omega$,

$$\varphi_x(x_i, y_j, t^n; \omega) = \frac{\phi^n_{i+1,j}(\omega) - \phi^n_{i-1,j}(\omega)}{2h_x} + \mathcal{O}(h_x^2), \tag{25}$$

$$u_x(x_i, y_j, t^n; \omega) = \frac{U^n_{i+1,j}(\omega) - U^n_{i-1,j}(\omega)}{2h_x} + \mathcal{O}(h_x^2), \tag{26}$$

$$u_{xx}(x_i, y_j, t^n; \omega) = \frac{U^n_{i+1,j}(\omega) - 2U^n_{i,j}(\omega) + U^n_{i-1,j}(\omega)}{2h_x} + \mathcal{O}(h_x^2). \tag{27}$$

Similar expressions can be derived for the m.s. spatial derivatives with respect to y.

To update the level set s.p. at each time level t^{n+1}, where $0 \le n \le N_t - 1$, we employ RPDEs (16)–(17), resulting in the following numerical approximation of the level set s.p., $\phi^{n+1}_{i,j}(\omega)$, $\omega \in \Omega$, for the interior points of the domain, where $1 \le i \le N_x - 1$ and $1 \le j \le N_y - 1$:

$$\begin{aligned} \phi^{n+1}_{i,j}(\omega) \ = \phi^n_{i,j}(\omega) - k\,\eta(\omega) & \sqrt{\left(\frac{U^n_{i+1,j}(\omega) - U^n_{i-1,j}(\omega)}{2h_x}\right)^2 + \left(\frac{U^n_{i,j+1}(\omega) - U^n_{i,j-1}(\omega)}{2h_y}\right)^2} \\ \times & \sqrt{\left(\frac{\phi^n_{i+1,j}(\omega) - \phi^n_{i-1,j}(\omega)}{2h_x}\right)^2 + \left(\frac{\phi^n_{i,j+1}(\omega) - \phi^n_{i,j-1}(\omega)}{2h_y}\right)^2}, \quad \omega \in \Omega. \end{aligned} \tag{28}$$

For any $\omega \in \Omega$, we recall that an acceptable difference scheme must converge to the partial differential equation as step sizes of the independent variables vanish. This property

called consistency requires that the truncation error vanishes as the discretization step sizes vanish, see Smith (1985).

The numerical scheme (28) for the free boundary update relies on central difference approximations for the spatial derivatives and a forward method for the temporal one. The truncation error, therefore, arises from the discretization in both time and space. This indicates that the method is first-order accurate in time and second-order accurate in space.

Once the habitat $\Phi(t^{n+1};\omega),\ \omega\in\Omega$, is defined, the numerical solution of the RPDE (2) can be calculated by explicit RFDS, denoted by REFDM:

$$U_{i,j}^{n+1}(\omega)=U_{i,j}^{n}(\omega)+kD(\omega)\frac{U_{i+1,j}^{n}(\omega)-2U_{i,j}^{n}(\omega)+U_{i-1,j}^{n}(\omega)}{h_x^2}$$
$$+\frac{U_{i,j+1}^{n}(\omega)-2U_{i,j}^{n}(\omega)+U_{i,j-1}^{n}(\omega)}{h_y^2}+U_{i,j}^{n}(\omega)\left(\alpha_{i,j}-\beta_{i,j}U_{i,j}^{n}(\omega)\right),\quad \omega\in\Omega, \tag{29}$$

for i and j such that $(x_i,\,y_j)\in\Phi(t^{n+1};\,\omega)$. In the scenario of finite degree of randomness and the involved variables having a truncated range, consistency of a random finite difference scheme is a consequence of the consistency of the underlying finite difference scheme for the deterministic case, see Casabán et al. (2021). Hence, the truncation error of the random explicit scheme (29) arises from discretizing both the spatial and temporal derivatives, introducing an error of $\mathcal{O}(k)+\mathcal{O}(h_x^2)+\mathcal{O}(h_y^2)$. The overall accuracy of the proposed method is determined by the combined truncation errors of the interior solver and the level set equation solver. Therefore, the method as a whole is first-order accurate in time and second-order accurate in space. This classic explicit scheme is straightforward to implement and conditionally stable. Moreover, as it will be shown further, the stability of the scheme depends on various factors, including the values of certain parameters, such as $D(\omega)$, that are randomly determined.

To enhance the stability properties of the random numerical algorithm, we adopt a deterministic explicit scheme proposed in Larkin (1964) for the random scenario resulting in the following

$$\left[z+D(\omega)(1+c^2)\right]U_{i,j}^{n+1}(\omega)=\left[z-D(\omega)(1+c^2)\right]U_{i,j}^{n}(\omega)$$
$$+D(\omega)\left(U_{i+1,j}^{n}(\omega)+U_{i-1,j}^{n+1}(\omega)\right)+D(\omega)c^2\left(U_{i,j+1}^{n}(\omega)+U_{i,j-1}^{n+1}(\omega)\right)$$
$$+h_x^2U_{i,j}^{n}(\omega)\left(\alpha_{i,j}-\beta_{i,j}U_{i,j}^{n}(\omega)\right),\quad \omega\in\Omega, \tag{30}$$

where $c=\frac{h_x}{h_y}$, $z=\frac{h_x^2}{k}$ and i and j such that $(x_i,\,y_j)\in\Phi(t^{n+1};\,\omega)$. This scheme is explicit, if both indexes are changing in ascending order. Therefore, we refer to it as RIEFDM (Random Improved Explicit Finite Difference Method). In the deterministic case of the linear diffusion equation, the sample scheme (30) for every single realization ω_ℓ, exhibits stability for any $z>0$ as reported in Larkin (1964). Due to the presence of a nonlinear term in RPDE (2), the unconditional stability is not guaranteed. In further section dedicated to the numerical analysis, we study the stability of this scheme demonstrating the conditional stability, but with less restrictive condition on step-sizes comparing with the REFDS (29).

Let us assume that $c=\frac{h_x}{h_y}$ is a constant. The m.s. consistency of the RIEFDM (30) with the RPDE (2) requires that $\frac{k}{h_x}$ tends to zero as h_x tends to zero. This fact is assured under the condition $z=\frac{h_x^2}{k}=$ const, allowing the scheme to accurately approximate the PDE.

With this condition in place, it can be shown that the truncation error of the scheme is $\mathcal{O}(h_x)$ assuming that z is a constant, see Larkin (1964).

Consistency can be enhanced by adopting the Random Average Larkin Alternating Direction Explicit (RALADE) method, based on Alternating Direction Explicit method proposed by Larkin (1964),

$$\begin{aligned}
&\left[2z + D(\omega)(1+c^2)\right] V_{i,j}^{n+1}(\omega) = \left[2z - D(\omega)(1+c^2)\right] U_{i,j}^{n}(\omega) \\
&\quad + D(\omega)\left(U_{i+1,j}^{n}(\omega) + V_{i-1,j}^{n+1}(\omega)\right) + D(\omega)c^2\left(U_{i,j+1}^{n}(\omega) + V_{i,j-1}^{n+1}(\omega)\right) \\
&\quad + h_x^2 U_{i,j}^{n}(\omega)\left(\alpha_{i,j} - \beta_{i,j} U_{i,j}^{n}(\omega)\right), \quad i,\ j \text{ in ascending order,} \qquad (31)\\
&\left[2z + D(\omega)(1+c^2)\right] Q_{i,j}^{n+1}(\omega) = \left[2z - D(\omega)(1+c^2)\right] U_{i,j}^{n}(\omega) \\
&\quad + D(\omega)\left(Q_{i+1,j}^{n+1}(\omega) + U_{i-1,j}^{n}(\omega)\right) + D(\omega)c^2\left(Q_{i,j+1}^{n+1}(\omega) + U_{i,j-1}^{n}(\omega)\right) \\
&\quad + h_x^2 U_{i,j}^{n}(\omega)\left(\alpha_{i,j} - \beta_{i,j} U_{i,j}^{n}(\omega)\right), \quad i,\ j \text{ in descending order,} \qquad (32)\\
&U_{i,j}^{n+1}(\omega) = \frac{V_{i,j}^{n+1}(\omega) + Q_{i,j}^{n+1}(\omega)}{2}, \quad \omega \in \Omega. \qquad (33)
\end{aligned}$$

Here, we employ two auxiliary random matrices to store the intermediate time-stepping results. As demonstrated in Larkin (1964), for the deterministic linear diffusion equation, the scheme (31)–(33) for a fixed realization ω_ℓ, is stable for any $z > 0$.

The RALADE scheme is absolutely consistent with the nonlinear problem (2), with a truncation error characterized by $\mathcal{O}(h_x^2) + \mathcal{O}\left(\frac{k^3}{h^2}\right) + \mathcal{O}(k)$. In particular, when the condition $z = \frac{h_x^2}{k} = \text{const}$ is satisfied, the truncation error simplifies to $\mathcal{O}(h_x^2)$. Therefore, the RALADE scheme enhances the overall performance and robustness in solving the RPDE.

Following Sect. 5 is focused in the analysis of positivity and stability of the numerical solution of the studied nonlinear diffusion–reaction problem for the three considered schemes.

5 Stability Analysis

The RFDS (29), (30) and (31)–(33) can be formulated using matrix notation as follows:

$$\mathbf{u}^{n+1}(\omega) = A(\omega) \cdot \mathbf{u}^{n}(\omega), \quad \omega \in \Omega, \qquad (34)$$

where $A(\omega)$ is a random matrix of coefficients of the corresponding RFDS, $\mathbf{u}^n(\omega)$ is a random vector of the numerical solution s.p. at n-th time level. In the case of two-dimensional problem, $\mathbf{u}^n(\omega)$ is a flattened version of the random matrix $U^n(\omega)$ preserving its column-wise structure in a one-dimensional vector format.

Now, we recall the definition of $\|\cdot\|_p$-stability in the fixed station sense of a random numerical scheme introduced in Casabán et al. (2021).

Definition 1 ($\|\cdot\|_p$-stability of a RFDS) A random numerical scheme (34) is said to be $\|\cdot\|_p$-stable in the fixed station sense in the domain $\Sigma \times [0,\ T]$, if for every partition with temporal step-size k defined in (20) and spatial step-sizes h_x and h_y, defined by (18) and (19), respectively, the p-norm of the r.v. $U_{i,j}^{n}(\omega)$, see (1), satisfies

$$\left\| U_{i,j}^{n}(\omega) \right\|_p \leq C, \quad 0 \leq n \leq N_t,\ 0 \leq i \leq N_x,\ 0 \leq j \leq N_y, \qquad (35)$$

where C is independent of the step-sizes and the time level n.

In the context of the sample-function approach, stability analysis is conducted on an individual basis for each realization within the stochastic framework. Each realization corresponds to a deterministic numerical scheme

$$\mathbf{u}^{n+1} = A \cdot \mathbf{u}^n, \tag{36}$$

transforming the inherently random problem into a collection of deterministic problems.

The core idea hinges on Definition 1, which provides the criteria for stability in the context of RFDS. Specifically, a random numerical scheme is deemed to be $\|\cdot\|_p$-stable in the fixed station sense if the deterministic numerical scheme (36) that arises by fixing each realization ω_ℓ adheres to a stability criterion introduced by Kröner (1997, p. 92), which relies on the infinity norm.

Definition 2 ($\|\cdot\|_\infty$-stability of a deterministic FDS) The sample numerical scheme (36) is said to be $\|\cdot\|_\infty$-stable in the fixed station sense in the computational domain, if for every partition with temporal step-size k defined in (20) and spatial step-sizes h_x and h_y, defined by (18) and (19), respectively, the sample infinite norm of the numerical solution $\mathbf{u}^n$ satisfies

$$\left\|\mathbf{u}^n\right\|_\infty = \max_{0\le m\le N_x N_y} |\mathbf{u}_m^n| = \max_{i,j} |U_{i,j}^n(\omega_\ell)| \le K \left\|\mathbf{u}^0\right\|_\infty, \quad 0 \le n \le N_t, \tag{37}$$

where $K > 0$ is some constant independent of time-level n and the step sizes h_x, h_y and k.

Indeed, if condition (37) is satisfied for any fixed realization $\omega_\ell \in \Omega$, then for any i, where $0 \le i \le N_x$, any j, where $0 \le j \le N_y$, and for any fixed level n, it follows that

$$|U_{i,j}^n(\omega_\ell)| \le \left\|\mathbf{u}^n\right\|_\infty \le K \left\|\mathbf{u}^0\right\|_\infty = K M_0, \tag{38}$$

where $M_0 = \max_{i,j} u_0(x_i, y_j)$ represents the maximum value of the initial condition (4) over the grid. Consequently,

$$\|U_{i,j}^n(\omega)\|_p = \left(\int_\Omega |U_{i,j}^n(\omega)|^p f_{U_{i,j}^n(\omega)} d\omega\right)^{1/p} \le K M_0 \left(\int_\Omega f_{U_{i,j}^n(\omega)} d\omega\right)^{1/p} = K M_0, \tag{39}$$

where $f_{U_{i,j}^n(\omega)}$ is the density function of $U_{i,j}^n(\omega)$ and therefore, $\int_\Omega f_{U_{i,j}^n(\omega)} d\omega = 1$. Taking in (39) $C = K M_0$, the p-norm of $U_{i,j}^n(\omega)$ is bounded by C, regardless of ω, step-sizes and time-level n.

Hence, in the remainder of this section, we focus on studying the stability of the numerical schemes (36) for a specific realization. This approach allows us to deduce the stability of the random numerical scheme (34) from analyzing the behavior of any of its sample schemes. Therefore, the argument ω is omitted.

5.1 Stability and positivity of the REFDM

To study the stability of the classical sample explicit Finite Difference Method (EFDM) defined by (29), we rewrite it in its sample version:

$$U_{i,j}^{n+1} = U_{i,j}^n \left[1 - \frac{2D(1+c^2)}{z} + k(\alpha_{i,j} - \beta_{i,j} U_{i,j}^n)\right]$$

$$+\frac{D}{z}\left(U^n_{i-1,j}+U^n_{i+1,j}+c^2(U^n_{i,j-1}+U^n_{i,j+1})\right), \tag{40}$$

where $c=\frac{h_x}{h_y}$ and $z=\frac{h_x^2}{k}$. In the sample EFDS (40), the matrix of coefficients, $A^n=A(\mathbf{u}^n)$, is dependent on $\mathbf{u}^n$, with non-diagonal entries being positive for any positive step-sizes, and the diagonal element for a fixed row, corresponding to the scheme at the (i,j)-grid point, is given by:

$$A^n_{q,q}=1-\frac{2D(1+c^2)}{z}+k(\alpha_q-\beta_q\mathbf{u}^n_q), \tag{41}$$

where sub-index $q=i+(j-1)N_y$ maps the two-dimensional spatial coordinates (i,j) to a singular dimension, signifying that the q-th row of the matrix A^n contains the coefficients of the finite-difference equation (40) at the (i,j)-grid point.

The following theorem states the conditions for the positivity and boundedness of the numerical solution $\mathbf{u}^n$ of (36), as well as for the stability of the sample EFDM (40).

Theorem 1 *Under the previous notation, the sample EFDM (40) is $\|\cdot\|_\infty$-stable in the sense of Definition 2, for all $n=0,\dots,N_t$, if the spatial and temporal step sizes, h_x and k, respectively, satisfy the condition*:

$$k<\frac{h_x^2}{2D(1+c^2)+Qh_x^2}, \tag{42}$$

where $Q=\max\left\{\kappa_1\left(2\frac{\kappa_2^2}{\kappa_1^2}-1\right);\ \kappa_2\left(2M_0-\frac{\kappa_1}{\kappa_2}\right)\right\}$, *being κ_1 and κ_2 defined in (7), and $M_0=\max_{i,j}u_0(x_i,y_j)$ denotes the maximum initial population density. Furthermore, under condition (42), the numerical solution $\mathbf{u}^n_q$ is positive and bounded as*:

$$0\le\mathbf{u}^n_q\le U_{\max},\quad U_{\max}=\max\{M_0,C_0\},\ \forall n=0,\dots,N_t, \tag{43}$$

where C_0 is the maximum carrying capacity defined by the following

$$C_0=\sup_{(x,y)\in\Phi_0}\frac{\alpha(x,y)}{\beta(x,y)},\quad \frac{\kappa_1}{\kappa_2}\le C_0\le\frac{\kappa_2}{\kappa_1}. \tag{44}$$

Proof of Theorem 1 The proof is based on the strategy proposed in Casabán et al. (2023).

Firstly, assuming $U_{\max}=C_0$, which corresponds to the case when $M_0\le C_0$. The principle of induction begins with $n=0$, where the initial condition $0\le\mathbf{u}^0_q\le M_0\le U_{\max}$ ensures positive diagonal elements $A^0_{q,q}$ under the constrain (42), as follows:

$$A^0_{q,q}=1-\frac{2D(1+c^2)}{z}+k(\alpha_q-\beta_q\mathbf{u}^0_q)\ge 1-k\left[\frac{2D(1+c^2)}{h_x^2}+\kappa_1\left(\frac{\kappa_2^2}{\kappa_1^2}-1\right)\right]>0, \tag{45}$$

which holds true since $Q\ge\kappa_1\left(\frac{\kappa_2^2}{\kappa_1^2}-1\right)$.

Since all coefficients of the sample scheme (40) are positive and $0\le\mathbf{u}^0_q\le M_0$, it directly implies $\mathbf{u}^1_q$ maintains positivity. In order to prove the boundedness of the solution $\mathbf{u}^1_q$, we use a similar idea to Casabán et al. (2023) that $\mathbf{u}^1_q$ can be considered as a function of $\mathbf{u}^0_q$, namely, $\mathbf{u}^1_q=f(\mathbf{u}^0_q)$ at each fixed grid point. Then the first derivative

$$\frac{\partial f}{\partial\mathbf{u}^0_q}=A^0_{q,q}-k\beta_q\mathbf{u}^0_q=1-\frac{2D(1+c^2)}{z}+k(\alpha_q-2\beta_q\mathbf{u}^0_q)>0,\ \text{if} \tag{46}$$

$$k < \frac{h_x^2}{2D(1+c^2) + h_x^2(2\beta_q \mathbf{u}_q^0 - \alpha_q)}, \quad \forall q. \tag{47}$$

Since

$$2\beta_q \mathbf{u}_q^0 - \alpha_q = \alpha_q \left(2\frac{\beta_q}{\alpha_q}\mathbf{u}_q^0 - 1\right) \leq \kappa_1 \left(2\frac{\kappa_2^2}{\kappa_1^2} - 1\right) \leq Q \quad \forall q, \tag{48}$$

condition (47) is fulfilled if k satisfies the hypothesis (42), which guarantees that the first derivative $\frac{\partial f}{\partial \mathbf{u}_q^0}$ is positive. Hence, $\mathbf{u}_q^1$ is an increasing function of $\mathbf{u}_q^0$, and for $0 \leq \mathbf{u}_q^0 \leq U_{\max}$, it follows:

$$\mathbf{u}_q^1 \leq f(C_0) = \left(1 + k\alpha_q \left(1 - \frac{C_0}{\alpha_q/\beta_q}\right)\right) C_0 \leq C_0 = U_{\max}, \tag{49}$$

which leads to the boundedness of $\mathbf{u}_q^1$.

For the inductive step, assuming $A_{q,q}^{n-1} > 0$ and $0 \leq \mathbf{u}_q^n \leq C_0$, now we demonstrate $A_{q,q}^n > 0$ and $0 \leq \mathbf{u}_q^{n+1} \leq C_0$. Since it is verified that $\mathbf{u}_q^{n+1} \leq C_0$, the positivity of $A_{q,q}^n$ holds under the hypothesis (42):

$$A_{q,q}^n = 1 - \frac{2D(1+c^2)}{z} + k(\alpha_q - \beta_q \mathbf{u}_q^n) \geq 1 - k\left[\frac{2D(1+c^2)}{h_x^2} + \kappa_1\left(\frac{\kappa_2^2}{\kappa_1^2} - 1\right)\right] > 0. \tag{50}$$

The positivity of the matrix A^n leads to the positivity of the vector $\mathbf{u}^{n+1}$ in the scheme (36). The boundedness of the solution is shown analogously to the base step by considering the solution at the next time moment as a function of the solution at the n-th time level, which finishes the proof for the first scenario when $M_0 \leq C_0$.

Now, let us consider the second scenario, when $M_0 \geq C_0$, i.e., when $U_{\max} = M_0$. Analogously to the previous case, the induction principle is used. At the base step, $n = 0$, the solution is bounded due to the initial conditions. Moreover,

$$M_0 \geq C_0 \geq \inf_{(x,y)\in\Phi_0} \frac{\alpha(x,y)}{\beta(x,y)} = \frac{\kappa_1}{\kappa_2}, \tag{51}$$

then

$$\alpha_q - \beta_q \mathbf{u}_q^0 \geq \alpha_q - \beta_q M_0 = \beta_q \left(\frac{\alpha_q}{\beta_q} - M_0\right) \geq \kappa_2 \left(\frac{\kappa_1}{\kappa_2} - M_0\right) = -\kappa_2 \left(M_0 - \frac{\kappa_1}{\kappa_2}\right). \tag{52}$$

Hence, under the condition (42), since $Q \geq \kappa_2 \left(M_0 - \frac{\kappa_1}{\kappa_2}\right)$, it holds that

$$A_{q,q}^0 = 1 - \frac{2D(1+c^2)}{z} + k(\alpha_q - \beta_q \mathbf{u}_q^0) \geq 1 - k\left[\frac{2D(1+c^2)}{h_x^2} + \kappa_2\left(M_0 - \frac{\kappa_1}{\kappa_2}\right)\right] > 0, \tag{53}$$

which also leads to the positivity of the solution $\mathbf{u}^1$. The boundedness is shown by using the same idea as in previous case. Let us consider the solution at the next time level as a function of the solution at current time level, i.e. $\mathbf{u}_q^1 = f(\mathbf{u}_q^0)$ at each fixed grid-point. Then the first derivative is positive under the constrain (42):

$$\frac{\partial f}{\partial \mathbf{u}_q^0} = A_{q,q}^0 - k\beta_q \mathbf{u}_q^0 = 1 - k\left[\frac{2D(1+c^2)}{h_x^2} + (2\beta_q \mathbf{u}_q^0 - \alpha_q)\right] > 0, \tag{54}$$

since $Q \geq h_x^2(2\kappa_2 M_0 - \kappa_1)$. Hence, $\mathbf{u}_q^1$ is increasing with respect to $\mathbf{u}_q^0$. Taking into account that $0 \leq \mathbf{u}_q^0 \leq M_0$, we get

$$\mathbf{u}_q^1 \leq f(M_0) \leq M_0 - k\alpha_q \left(\frac{M_0}{\alpha_q/\beta_q} - 1 \right) M_0 \leq M_0. \tag{55}$$

At the inductive step, we assume that $A_{q,q}^{n-1} > 0$ and all $\mathbf{u}_q^n$ are positive and $\mathbf{u}_q^n \leq M_0$. Let us show that $A_{q,q}^n > 0$ and $0 \leq \mathbf{u}_q^{n+1} \leq M_0$. The positivity of $A_{q,q}^n$ holds under the hypothesis (42):

$$\begin{aligned} A_{q,q}^n &= 1 - \frac{2D(1+c^2)}{z} + k(\alpha_q - \beta_q \mathbf{u}_q^n) \\ &\geq 1 - k\left[\frac{2D(1+c^2)}{h_x^2} + \kappa_2 \left(M_0 - \frac{\kappa_1}{\kappa_2} \right) \right] > 0, \end{aligned} \tag{56}$$

thereby confirming $A_{q,q}^n > 0$ under the specified conditions, and by extension. The positivity of the matrix A^n leads to the positivity of the vector $\mathbf{u}^{n+1}$ in the scheme (36), hence the positivity and boundedness of $\mathbf{u}_q^{n+1}$ through analogous logic applied in the previous case. □

Applying the results of the Theorem 1 to the random case, the following result can be established.

Corollary 1 *Given the previous notation and considering the boundedness of the random parameter $D(\omega)$ as provided in (6), the REFDM (29) is $\|\cdot\|_p$-stable in the fixed station sense for all $n = 0, \ldots, N_t$, $\omega \in \Omega$, and the numerical solution s.p. is bounded as follows*:

$$0 \leq \mathbf{u}_q^n(\omega) \leq U_{\max}, \quad \textit{for } \omega \in \Omega, \tag{57}$$

provided that the following condition holds:

$$k < \frac{h_x^2}{2d_2(1+c^2) + Qh_x^2}. \tag{58}$$

For the rest of methods, we use similar approach.

5.2 Stability and positivity of the RIEFDM

In this subsection, we study the stability of the RIEFDM (30), which is unconditionally stable for the linear diffusion equation case, as shown in Larkin (1964). For a particular ω_ℓ, the scheme (30) is rewritten in the following form

$$\begin{aligned} &\left[z + D(1+c^2)\right] U_{i,j}^{n+1} - DU_{i-1,j}^{n+1} - Dc^2 U_{i,j-1}^{n+1} \\ &\quad = \left[z - D(1+c^2) + h_x^2 \left(\alpha_{i,j} - \beta_{i,j} U_{i,j}^n \right) \right] U_{i,j}^n + DU_{i+1,j}^n + Dc^2 U_{i,j+1}^n, \end{aligned} \tag{59}$$

and denoted by IEFDM as a sample of RIEFDM. The scheme (59) in matrix form is given by

$$F \cdot \mathbf{u}^{n+1} = B^n \cdot \mathbf{u}^n, \tag{60}$$

where $\mathbf{u}^n = \{U_{i,j}^n\}$ is a vector containing all grid values, F is a lower-triangular matrix of constant coefficients on the left-hand side, and $B^n = B(\mathbf{u}^n)$ is an upper-triangular matrix

of coefficients on the right-hand side. Moreover, since off-diagonal entries of F are all non-positive, F is a M-matrix, and therefore inverse-positive: $\exists F^{-1}$ and $F^{-1} \geq 0$, see Plemmons (1977). Since the product of two non-negative matrices is non-negative, $A^n = F^{-1}B^n \geq 0$, if $B^n \geq 0$. The non-diagonal entries of B are positive due to the non-negativity of the diffusion coefficient D. So, the positivity of the numerical solution $\mathbf{u}^n$ is guaranteed if the diagonal entries of the matrix B^n are all non-negative at each time level n. The following theorem established the conditions for the positivity and stability of the proposed numerical scheme (59).

Theorem 2 *With previous notation, the numerical scheme (60) is stable if the spatial and temporal step sizes, h_x and k, respectively, satisfy the condition*

$$k < \frac{h_x^2}{D(1+c^2) + h_x^2(2\kappa_2 U_{\max} - \kappa_1)}. \tag{61}$$

Under (61), the numerical solution $\mathbf{u}_q^n$ is bounded as follows:

$$0 \leq \mathbf{u}_q^n \leq U_{\max}. \tag{62}$$

Proof of Theorem 2 We apply the principle of induction. At the base step, when $n = 0$, one gets

$$B_{q,q}^0 = z - D(1+c^2) + h_x^2\left(\alpha_q - \beta_q \mathbf{u}_q^0\right), \tag{63}$$

which is positive under condition (61). Indeed, in the worth case, when $(\alpha_q - \beta_q \mathbf{u}_q^0) < 0$, one gets

$$B_{q,q}^0 = z - D(1+c^2) - h_x^2\left(\beta_q \mathbf{u}_q^0 - \alpha_q\right) > 0, \quad \text{if} \tag{64}$$

$$\frac{h_x^2}{k} > D(1+c^2) + h_x^2\left(\beta_q \mathbf{u}_q^0 - \alpha_q\right) > 0. \tag{65}$$

By taking into account the bounds (7), the definition of $U_{\max}$, and the following bound

$$h_x^2(\beta_q \mathbf{u}_q^0 - \alpha_q) \leq h_x^2(\kappa_2 U_{\max} - \kappa_1), \tag{66}$$

we obtain that $B_{q,q}^0 > 0$ if

$$k < \frac{h_x^2}{D(1+c^2) + h_x^2(\kappa_2 U_{\max} - \kappa_1)}, \tag{67}$$

which is fulfilled under the condition (61). Hence, the positivity of $\mathbf{u}^1$ is guaranteed.

The boundedness of the numerical solution $\mathbf{u}^0$ leads from the initial conditions. To show that $\mathbf{u}_q^1 \leq U_{\max}\ \forall q$, we employ the similar strategy as in the study of the stability of the EFDM above. Let us consider $\mathbf{u}_q^1 = f(\mathbf{u}_q^0)$, using explicit form (59):

$$\begin{aligned}\mathbf{u}_q^1 = &\frac{\left(z - D(1+c^2) + h_x^2\left(\alpha_q - \beta_q \mathbf{u}_q^0\right)\right)\mathbf{u}_q^0}{z + D(1+c^2)} \\ &+ \frac{D(\mathbf{u}_{q+1}^0 + \mathbf{u}_{q-1}^1) + Dc^2(\mathbf{u}_{q+N_y}^0 + \mathbf{u}_{q-N_y}^1)}{z + D(1+c^2)}.\end{aligned} \tag{68}$$

Note that in (59) terms with $\mathbf{u}^1_{q-1}$ and $\mathbf{u}^1_{q-Ny}$ also depend on $\mathbf{u}^0_q$. Hence, the first derivative is given by

$$\frac{\partial f}{\partial \mathbf{u}^0_q} = \frac{1}{z + D(1+c^2)} \left[z - D(1+c^2) + h_x^2(\alpha_q - 2\beta_q \mathbf{u}^0_q) + \frac{D^2(1+c^4)}{z + D(1+c^2)} \right]. \quad (69)$$

Since $\frac{D^2(1+c^4)}{z+D(1+c^2)} > 0$, the following estimation takes place

$$\frac{\partial f}{\partial \mathbf{u}^0_q} > \frac{1}{z + D(1+c^2)} \left[z - D(1+c^2) + h_x^2(\alpha_q - 2\beta_q \mathbf{u}^0_q) \right] > 0, \quad \text{if} \quad (70)$$

$$k < \frac{h_x^2}{D(1+c^2) + h_x^2(2\beta_q \mathbf{u}^0_q - \alpha_q)}, \quad \forall q, \quad (71)$$

which is fulfilled under condition (61). Hence, $\mathbf{u}^1_q$ is increasing with respect to $\mathbf{u}^0_q$ and the following bound can be established:

$$\mathbf{u}^1_q \le f(U_{\max}) = \left[1 - \frac{h_x^2}{z + D(1+c^2)} \left(\beta_q U_{\max} - \alpha_q \right) \right] U_{\max} \le U_{\max}, \quad (72)$$

due to the fact that $U_{\max} \ge C_0$.

By induction, analogously to the case of EFDM, if the spatial and temporal discretization parameters satisfy (61), the IEFDM scheme (59) is found to be stable, and the numerical solution remains within the bounds of 0 and $U_{\max}$ for all n. □

It is important to observe that while the scheme delineated by (59) demonstrates unconditional stability (Larkin 1964), for linear diffusion equations, the nonlinearity of the source term introduces complexity into the stability analysis, requiring more stringent restrictions on the step-sizes. However, the stability conditions for the classical EFDM (40) specified in (42) impose stricter constraints compared to those required for the IEFDM (59) as specified in (61).

Corollary 2 *With previous notation, the RIEFDM (30) is $\|\cdot\|_p$-stable in the fixed station sense, and preserves positivity and boundedness of the numerical solution s.p. as follows*

$$0 \le \mathbf{u}^n_q(\omega) \le U_{\max}, \quad (73)$$

for all $n = 0, \dots, N_t$, $\omega \in \Omega$, under the following step-sizes condition

$$k < \frac{h_x^2}{d_2(1+c^2) + h_x^2(2\kappa_2 U_{\max} - \kappa_1)}. \quad (74)$$

The deterministic case of the scheme (31)–(33) is denoted by ALADE and written as follows

$$\begin{aligned}
&\left[2z + D(1+c^2)\right] V^{n+1}_{i,j} = \left[2z - D(1+c^2)\right] U^n_{i,j} \\
&\quad + D\left(U^n_{i+1,j} + V^{n+1}_{i-1,j}\right) + Dc^2\left(U^n_{i,j+1} + V^{n+1}_{i,j-1}\right) \\
&\quad + h_x^2 U^n_{i,j}\left(\alpha_{i,j} - \beta_{i,j} U^n_{i,j}\right), \quad i,\ j \text{ in ascending order}, \\
&\left[2z + D(1+c^2)\right] Q^{n+1}_{i,j} = \left[2z - D(1+c^2)\right] U^n_{i,j} \\
&\quad + D\left(Q^{n+1}_{i+1,j} + U^n_{i-1,j}\right) + Dc^2\left(Q^{n+1}_{i,j+1} + U^n_{i,j-1}\right)
\end{aligned} \quad (75)$$

$$+h_x^2 U_{i,j}^n \left(\alpha_{i,j} - \beta_{i,j} U_{i,j}^n\right), \quad i,\ j \text{ in descending order,} \tag{76}$$

$$U_{i,j}^{n+1} = \frac{V_{i,j}^{n+1} + Q_{i,j}^{n+1}}{2}. \tag{77}$$

Performing similar analysis on the schemes (31)–(33) and (75)–(77) results in the following theorem.

Theorem 3 *With previous notation, the RALADE* (31)–(33) *is* $\|\cdot\|_p$*-stable in the fixed station sense, if*

$$k < \frac{2h_x^2}{d_2(1+c^2) + h_x^2(2\kappa_2 U_{\max} - \kappa_1)}. \tag{78}$$

Moreover, if (78) *is fulfilled, the numerical solution s.p.* $\mathbf{u}_q^n(\omega)$, $\omega \in \Omega$, *is non-negative and bounded by* $U_{\max}$.

Therefore, the proposed numerical schemes ensure stability, positivity, and boundedness of the numerical solution s.p. upon specific conditions related to step sizes. Notably, the RALADE scheme (31), is the least restrictive among all the proposed schemes. This scheme consistently demonstrates stability across all simulations conducted in the subsequent section, underscoring its robustness and efficiency.

6 Numerical algorithm

Addressing the storage problems associated with computing the expectation and variance of the approximate solution s.p. by the RLSM and RFDS developed above, we employ a combination of the sample m.s. approach with the Monte Carlo method.

In our approach, we generate a specified number K of realizations for the random parameters involved in the RPDE (2)–(5), and compute the numerical solutions for each realization ω_ℓ at time horizon $[0, T]$, $\left\{U^{N_t}(\omega_\ell),\ 1 \le \ell \le K\right\}$. All the steps to compute stable numerical approximations for RPDE problem (2)–(5) for every fixed realization ω_ℓ, are summarized in Algorithm 1.

The following step is to compute the mean and standard deviation of the numerical solution s.p. simultaneously, using the well-known formulae:

$$\mu[U^{N_t}] = \frac{1}{K}\sum_{\ell=1}^{K} U^{N_t}(\omega_\ell), \quad \sigma[U^{N_t}] = \sqrt{\frac{1}{K}\sum_{\ell=1}^{K}\left(U^{N_t}(\omega_\ell)\right)^2 - \left(\mu[U^{N_t}]\right)^2}. \tag{79}$$

Algorithm 2 provides an overview of the procedure for efficient computing the statistical moments of the numerical solution s.p. for the RPDE problem (2)–(5).

In order to enhance the computational efficiency, especially when dealing with large-scale Monte Carlo simulations, we have implemented a parallel computing environment. This approach enables each processor to independently compute the numerical solutions for each realization of the random variables. By simultaneously executing computations across multiple processors, we can significantly improve the efficiency and speed of Monte Carlo simulations.

For parallel computing, MATLAB provides a specialized tool known as the Parallel Computing Toolbox. This toolbox includes an improved variant of the `for` loop, referred to as

Algorithm 1 Random Level Set Method for Random Logistic Diffusion Problem for fixed $\omega_\ell \in \Omega$

Require: $D(\omega_\ell)$, $\eta(\omega_\ell)$, $\alpha(x, y)$, $\beta(x, y)$, T, $U_0(x, y)$, Φ_0, N_x, N_y, $x_{\min}, x_{\max}, y_{\min}, y_{\max}$

1: Define uniform grid (x_i, y_j) by (18)–(19)
2: Choose the RFDS: REFDM (29), RIEFDM (30) or RALADE (31)–(33)
3: Set k verifying stability conditions (58), (74) or (78), respectively
4: $N_t \leftarrow$ number of time levels to achieve T
5: Set initial conditions by (21)
6: Compute $\phi^0_{i,j}(\omega_\ell)$ by (22)
7: **for** $n = 0$ to $N_t - 1$ **do**
8: Update the level set function by (28)
9: Update the solution $\tilde{U}^{n+1}_{i,j}(\omega_\ell)$ by using one of the explicit methods (29), (30) or (31)–(33)
10: Update the
11: Define free boundary at $(n + 1)$ time level:

$$U^{n+1}_{i,j}(\omega_\ell) = \begin{cases} \tilde{U}^{n+1}_{i,j}(\omega_\ell), & \text{if } \phi^{n+1}_{i,j}(\omega_\ell) < 0, \\ 0, & \text{otherwise} \end{cases}$$

12: Enforce boundary conditions on the level-set function:

$$\nabla\varphi(x_i, y_j, t^{n+1};\ \omega_\ell) = 0, \quad \forall (x_i, y_j) \in \partial\Sigma$$

13: **end for**

Algorithm 2 Monte Carlo technique for computing the statistical moments of the numerical solution s.p. for RPDE problem (2)–(5)

Require: K

1: SUM $\leftarrow 0$
2: SUM2 $\leftarrow 0$
3: **for** each realization ω_ℓ, $1 \le \ell \le K$ **do**
4: Set r.v. parameters $D(\omega_\ell)$ and $\eta(\omega_\ell)$ for the problem (2)–(5)
5: $U^{N_t}(\omega_\ell) \leftarrow$ numerical solution of (2)–(5) for ω_ℓ by Algorithm 1
6: SUM $\leftarrow$ SUM $+ U^{N_t}(\omega_\ell)$
7: SUM2 $\leftarrow$ SUM2 $+ \left(U^{N_t}(\omega_\ell)\right)^2$
8: **end for**
9: $\mu[U^{N_t}] \leftarrow$ SUM$/K$
10:
11: $\sigma[U^{N_t}] \leftarrow \sqrt{\text{SUM2}/K - \left(\mu[U^{N_t}]\right)^2}$

`parfor`. This function enables iterations of a particular code block to be executed a specified number of times in parallel, thus offering a practical and efficient way to leverage the advantages of parallel computing in Monte Carlo simulations.

7 Results and discussion

Computation have been carried out by Matlab© software version R2024a for Windows 11 (64-bit), processor 11th Gen Intel(R) Core(TM) i5-11300H @ 3.10 GHz 3.11 GHz.

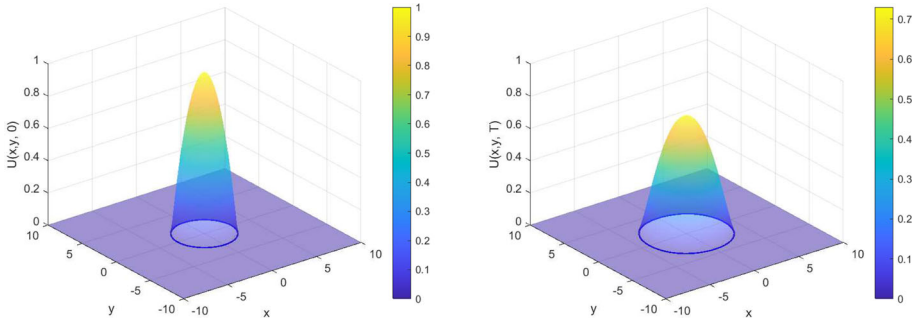

Fig. 1 Initial (left) and final at $T = 3$ (right) population distribution for Example 1 using LSM with ALADE

7.1 Deterministic case

In this section, we present numerical results for a deterministic case, where we consider a single fixed realization $\omega_\ell \in \Omega$. As it was mentioned in Sect. 2, the m.s. approach has the property that the m.s. solution coincides with the one obtained in the deterministic case. These examples aim to compare the proposed methods with other established (Casabán et al. 2024), as well as to explore the stability and other qualitative properties studied above.

Example 1 Model with radial symmetry (Casabán et al. 2023)

We consider a simplified version of the model delineated by (2)–(4), which is characterized by radial symmetry. The free boundary logistic diffusive 1D model introduced in Du and Lin (2010) was extended for the multidimensional case with radial symmetry in Du and Guo (2011). By adopting this assumption, we can reduce the general multidimensional PDE to a one-dimensional variant with a singular spatial variable, denoted as $r = |x|$, where $x \in \mathbb{R}^N$. Within the scope of this paper, our focus is on the case where $N = 2$, indicating a two-dimensional problem.

We examine the model with radial symmetry on the initial habitat $\Phi_0 = \{(x, y) \in \mathbb{R}^2 : x^2 + y^2 \leq H_0^2\}$, where $H_0 = 3$ with the following parameters

$$D = 1,\ \eta = 2,\ T = 3,\ u_0(x, y) = 1 - \frac{x^2 + y^2}{H_0^2}. \tag{80}$$

The parameters $\alpha = 1$ and $\beta = 1$ are chosen to be constant for simplicity.

In this Example, we define the computational domain as $[-10,\ 10] \times [-10,\ 10]$ to guarantee the caption of the front growth. We set the grid resolution to $N_x = N_y = 200$, ensuring a fine-grained representation of the domain. The time step for the ALADE (75)–(77) is defined as $k = h^2$, where $h = \min\{h_x,\ h_y\}$.

The initial condition for the level set function, $\varphi(x, y)$, is given by

$$\varphi(x, y, 0) = \sqrt{x^2 + y^2} - H_0. \tag{81}$$

This formulation ensures that the level set function is negative within the circle Φ_0, zero at the boundary of Φ_0, and positive outside Φ_0.

The initial and final population distributions (at $t = T$) are depicted in Fig. 1. The considered method is shown to preserve the radial symmetry as shown in Fig. 2. These results agree with those previously published in Casabán et al. (2024), obtained using the front-fixing and front-tracking methods, see Fig. 3.

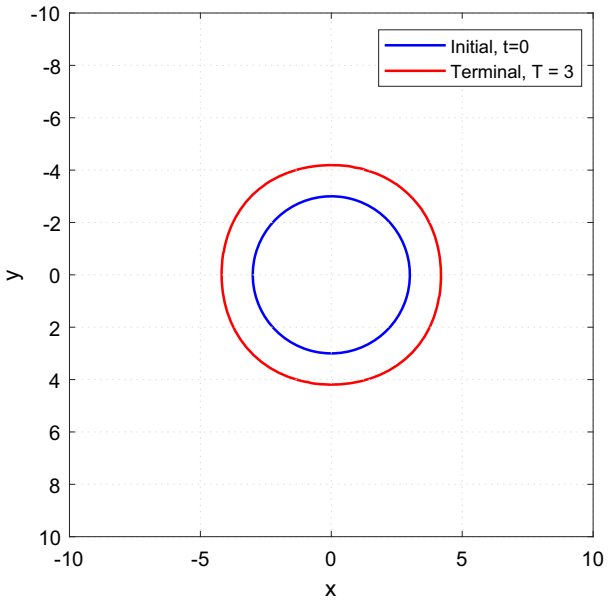

Fig. 2 Evolution of the front for Example 1

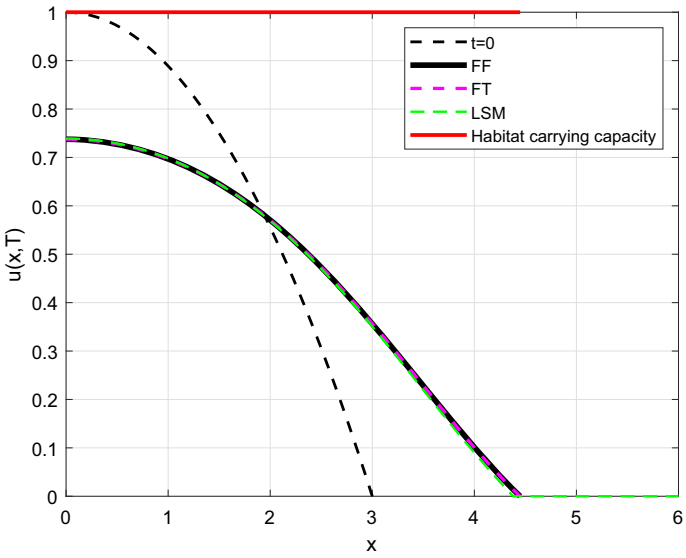

Fig. 3 Comparison of the proposed method (LSM with ALADE) versus front-fixing (FF) and front-tracking (FT) methods for Example 1

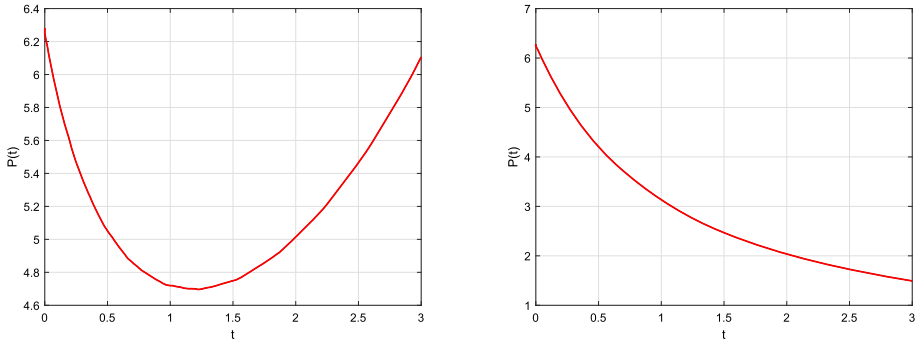

Fig. 4 Spreading-vanishing dichotomy in Example 1 with $H_0 = 2$: spreading for $\eta_1 = 2$ (left), vanishing for $\eta_2 = 0.2$ (right)

In order to measure the population in the habitat, the following formula is used

$$P(t) = \iint_{\Phi(t)} u(x, y, t)\, dx\, dy. \tag{82}$$

In this case, the spreading is observed, since the initial population, $P(0) = 14.1363$ increases to the final value $P(T) = 19.3690$, which agrees with previous results.

Based on the previous study of the spreading-vanishing dichotomy, as presented in Theorem 2 of Casabán et al. (2023), when the initial habitat is too small ($H_0 < R^* = 2.4048$, for the parameters (80)) and the front expanding rate η is insufficient for propagation ($\eta < \eta^*$), the population vanishes. In this other study, now we set $H_0 = 2$, leading to the corresponding threshold value of η as $\eta^* = 0.2682$. Figure 4 displays the population growth computed using formula (82) for two different values of η: $\eta_1 = 2 > \eta^*$ and $\eta_2 = 0.2 < \eta^*$. The results clearly demonstrate that the proposed LSM method combined with ALADE preserves the spreading-vanishing dichotomy in the multi-dimensional case.

Example 2 Stability and numerical convergence of the proposed FDS.

It is well-established that traditional explicit schemes exhibit conditional stability, often requiring use of smaller time steps and consequently leading to prolonged computational time. This limitation becomes extremely important in RPDE solvers, where the application of the Monte Carlo method results in a multiplication of computational time by the number of realizations.

However, the IEFDM (59) and ALADE (75)–(77) methods have demonstrated superior stability characteristics, as illustrated in Sect. 5. Let us confirm this with the model in Example 1. In Fig. 5, we present population dynamics over time using various time steps keeping spatial step sizes fixed ($N_x = N_y = 200$). Solid lines depict solutions meeting the stability condition for each method ($k = k^*$), while dashed lines indicate solutions where the stability condition is broken: for EFDM (40), we set $k = 1.01k^*$, and for IEFDM and ALADE, $k = 1.5k^*$. In the case of EFDM, such a slight increment causes the solution to begin losing stability, leading to the emergence of negative population values. Hence, we numerically highlight the significance of the derived stability condition (42) and its strong sensitivity. Conversely, IEFDM (59) and ALADE (75)–(77) exhibit less sensitivity to the stability condition.

We also evaluate the convergence of both the IEFDM and ALADE methods. To ensure consistency in the IEFDM scheme, it is essential that the condition $z = \frac{h_x^2}{k} = \text{const}$ is satisfied.

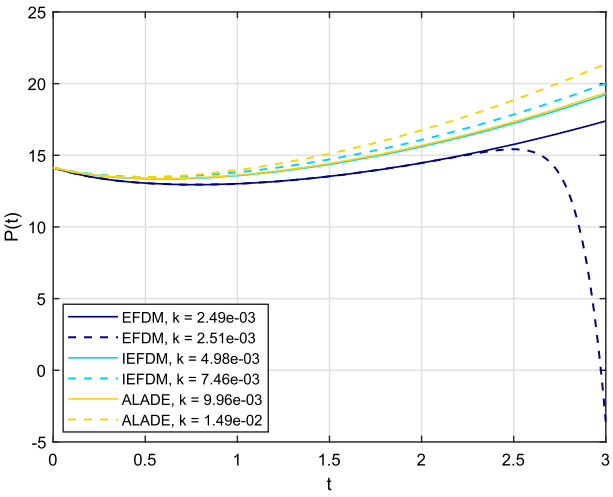

Fig. 5 Stability of the methods for Example 2: solid lines depict solutions meeting the stability condition; dashed lines indicate solutions where the stability condition is broken

To this end, we conduct a series of tests where the spatial discretization is uniformly applied, setting $h_x = h_y = h_m$. The spatial grid sizes are defined as $h_m = 0.05 \times 2^m$ for $m = 0, \ldots, 4$, with the corresponding time steps given by $k_m = h_m^2$.

As the exact solution is not known, we define the mean squared error (MSE) in terms of the following mean square successive deviations:

$$\mathrm{MSE}(h_m, h_{m+1}) = \frac{1}{(N_x+1)(N_y+1)} \sum_{j=0}^{N_y} \sum_{i=0}^{N_x} |U_{i,j}^{N_t}(h_m) - U_{i,j}^{N_t}(h_{m+1})|^2, \tag{83}$$

where $U_{i,j}^{N_t}(h_m)$ is the numerical solution at the node (x_i, y_j) at the moment $t = T$ computed by the numerical scheme with step sizes $h_x = h_y = h_m$ and $k = h_m^2$. The errors associated with the IEFDM and ALADE methods are depicted in Fig. 6.

Next, we calculate the convergence rate γ as follows

$$\gamma(h_m, h_{m+1}, h_{m+2}) = \frac{\ln|\mathrm{MSE}(h_{m+1}, h_{m+2})| - \ln|\mathrm{MSE}(h_m, h_{m+1})|}{\ln 2}. \tag{84}$$

The mean convergence rate γ for the IEFDM method is 1.53, while the mean convergence rate for the ALADE scheme is 2.02. These results align with the theoretical predictions regarding truncation error, demonstrating the efficacy of both methods in achieving convergence.

As a result, in forthcoming examples with random parameters, we will exclude the REFDM (40) scheme from consideration and focus primarily on the RALADE method (31)–(33). This choice is made due to the RALADE method's experimental characteristics being equivalent to those of the RIEFDM, while it theoretically converges more rapidly. To evaluate the effectiveness of the proposed RLSM with RALADE method, we conduct tests in a random scenario without making any assumptions about radial symmetry. This approach enables us to scrutinize the method's performance in scenarios where radial symmetry cannot be assumed.

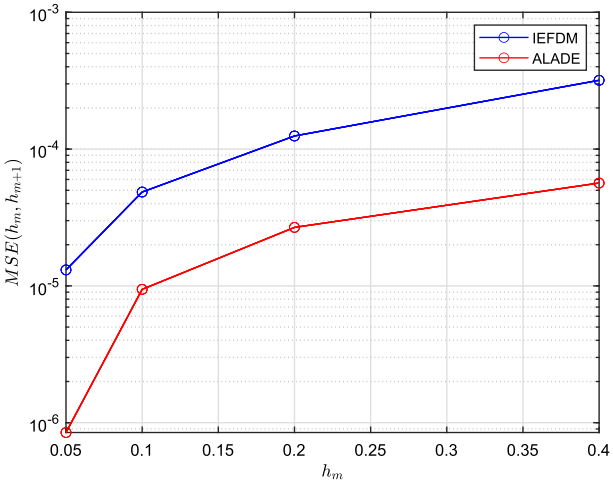

Fig. 6 Mean squared error (83) of the IEFDM and ALADE methods

Table 1 Mean squared error (83) of the IEFDM and ALADE methods

h_m	MSE(h_m, h_{m+1}) of $\mu[U^{N_t}]$		MSE(h_m, h_{m+1}) of $\sigma[U^{N_t}]$	
	RIEFDM	RALADE	RIEFDM	RALADE
0.05	1.2001e−05	6.8849e−07	3.0950e−07	6.1662e−08
0.1	4.9623e−05	9.8571e−06	1.2449e−06	2.9888e−07
0.2	1.1018e−04	2.7565e−05	9.8503e−06	1.5919e−06
0.4	2.2176e−04	3.7393e−05	5.2915e−05	5.6947e−06

7.2 Random case: numerical convergence and variability

First, we replicate the previous experiment to investigate the numerical convergence of the proposed RFDS.

Example 3 Numerical convergence of the RFDS.

Let us consider the RPDE problem (2)–(5) with $T = 3$, $\alpha = 1$, $\beta = 1$, and the random parameters

$$D(\omega) \sim \mathcal{N}_{[0.8,\,1.2]}(1,\,0.1), \quad \eta(\omega) \sim \mathcal{B}e_{[1.6,\,2.4]}(2;\,4), \tag{85}$$

that is, $D(\omega)$ follows a normal distribution of mean $\mu = 1$ and the standard deviation $\sigma = 0.1$, truncated on the interval $[0.8,\ 1.2]$; $\eta(\omega)$ has a shifted-beta distribution of parameters $(2;\ 4)$ with a support from 1.6 to 2.4. We set the number of Monte Carlo simulations to $K = 100$. The mean squared error (MSE) is calculated for both the RIEFDM and the RALADE methods using formula (83). However, instead of using the numerical solution $U_{i,j}^{N_t}(h_m)$, we compute the MSE based on the mean value and standard deviation obtained from the K simulations. The results are presented in Table 1. The mean convergence rate γ, computed using formula (84), is found to be 1.40 for the RIEFDM method and 1.92 for the RALADE scheme. These findings are consistent with previous results obtained for the deterministic case.

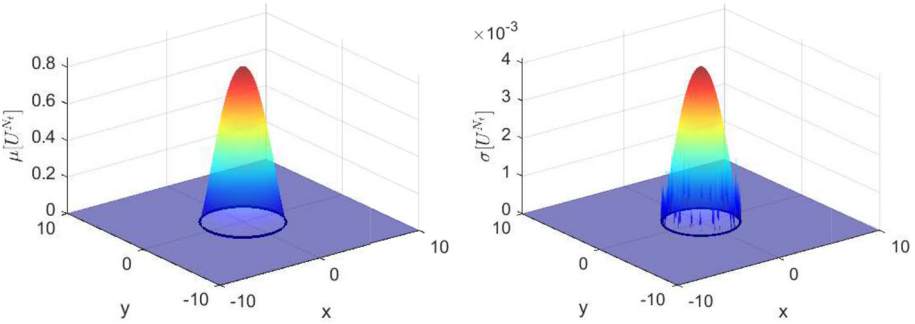

Fig. 7 Mean (left) and standard deviation (right) of the numerical solution s.p.'s at $T = 1$ for Example 4, for $K = 800$

The following example presents a study of the numerical convergence of the proposed RLSM method combined with the RALADE technique.

We fix the initial area and normalize the initial population density to ensure that at $t = 0$, it is equal to 1, as follows:

$$U_0(x, y) = \frac{u_0(x, y)}{P(0)}. \tag{86}$$

Example 4 Numerical convergence of the Monte Carlo simulations.

Let us consider the RPDE problem (2)–(5) with $T = 1$, and rest of the parameters from the previous Example 3. We set the number of spatial step-sizes $N_x = N_y = 200$, and set the number of simulations $K = 800$. The statistical moments for the numerical solution s.p. are presented in Fig. 7: in the left panel the mean is presented, and the standard deviation is plotted in the right panel. As expected, the standard deviation is higher where the mean is higher.

Now, let us consider the results for various number of samples for the Monte Carlo method. The expected values of the fronts for different K are plotted in Fig. 8. The right plot presents a zoom of the left plot. As observed, the fronts are indistinguishable, which implies that the Monte Carlo method adequately captures the behavior of the system even with a small number of realizations K without substantial variations in the resulting fronts.

To analyze the numerical convergence, we introduce the following pairwise error measures:

$$\varepsilon_{K_1, K_2}(\mu[U^{N_t}]) = \left|\mu_{K_1}[U^{N_t}] - \mu_{K_2}[U^{N_t}]\right|, \tag{87}$$

$$\varepsilon_{K_1, K_2}(\sigma[U^{N_t}]) = \left|\sigma_{K_1}[U^{N_t}] - \sigma_{K_2}[U^{N_t}]\right|, \tag{88}$$

where $\mu_K[U^{N_t}]$ is the mean and $\sigma_K[U^{N_t}]$ is the standard deviation at $T = 1$ computed by the Algorithm 2 for K samples. The infinite norm of the errors is reported in Table 2.

Example 5 Variability of the numerical solution s.p.

In this example, we investigate how the dispersion of the random parameters affects variability of the samples of the numerical solution s.p. We consider the RPDE problem with parameters defined in Example 4. To estimate the impact from the dispersion of the random parameter $\eta(\omega)$, we perform $K = 100$ Monte Carlo simulations with a fixed diffusion

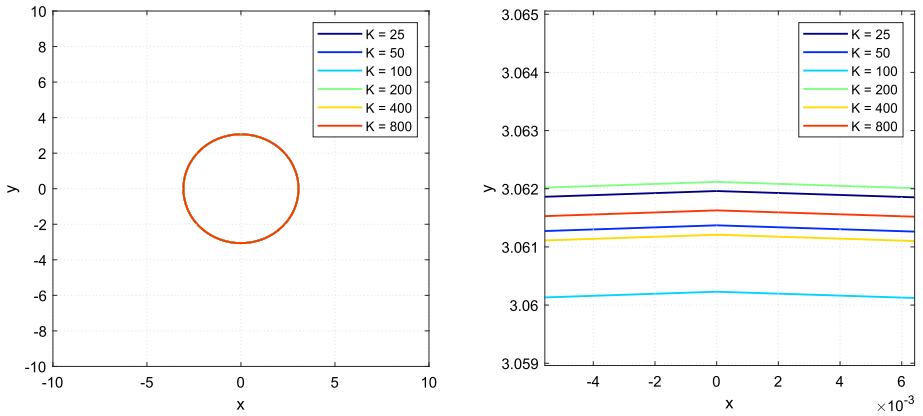

Fig. 8 The mean of the fronts at $T = 1$ for varying numbers of samples K in the Monte Carlo method for Example 4

Table 2 Infinite norm of the pairwise error measure (87)–(88) for the numerical solution s.p. of Example 4

$\{K_1,\ K_2\}$	$\left\|\varepsilon_{K_1,\,K_2}(\mu[U^{N_t}])\right\|_\infty$	$\left\|\varepsilon_{K_1,\,K_2}(\sigma[U^{N_t}])\right\|_\infty$
{25, 50}	2.4282e−02	1.3450e−02
{50, 100}	2.2753e−02	4.0889e−02
{100, 200}	3.5122e−03	2.8235e−02
{200, 400}	4.1622e−02	1.5423e−03
{400, 800}	2.9250e−02	6.3869e−03

coefficient $D = 1$. We consider two scenarios: $\eta_1(\omega) \sim \mathcal{B}e_{[1.6,\,2.4]}(2;\,4)$, and $\eta_2(\omega) \sim \mathcal{B}e_{[1.6,\,2.4]}(200;\,400)$. The mean of a shifted beta distribution $\mathcal{B}e_{[a,b]}(\alpha,\,\beta)$ is calculated as follows

$$\mathbb{E}[\eta_1(\omega)] = a + (b-a)\frac{\alpha}{\alpha+\beta} = 1.6 + 0.8\frac{2}{6} = 1.87, \quad \mathbb{E}[\eta_2(\omega)] = 1.87. \tag{89}$$

Hence, while expected values of both distributions are the same, their standard deviations differ:

$$\sigma[\eta_1(\omega)] = (b-a)\sqrt{\frac{\alpha\beta}{(\alpha+\beta)^2(\alpha+\beta+1)}} = 0.14, \quad \sigma[\eta_2(\omega)] = 0.015. \tag{90}$$

Figure 9 compares the population samples in both scenarios.

We now repeat the experiment for the normal distribution. We fix $\eta = 2$ for all $K = 100$ simulations and consider two scenarios: $D_1(\omega) \sim \mathcal{N}_{[0.8,\,1.2]}(1,\,0.1)$ and $D_2(\omega) \sim \mathcal{N}_{[0.8,\,1.2]}(1,\,0.01)$. Results are plotted in Fig. 10. As expected, increasing the standard deviation σ of the random parameter $D(\omega)$ leads to a wider spread in the samples of the numerical solution. Furthermore, the case with $\sigma = 0.1$ shows the presence of a spreading-vanishing dichotomy.

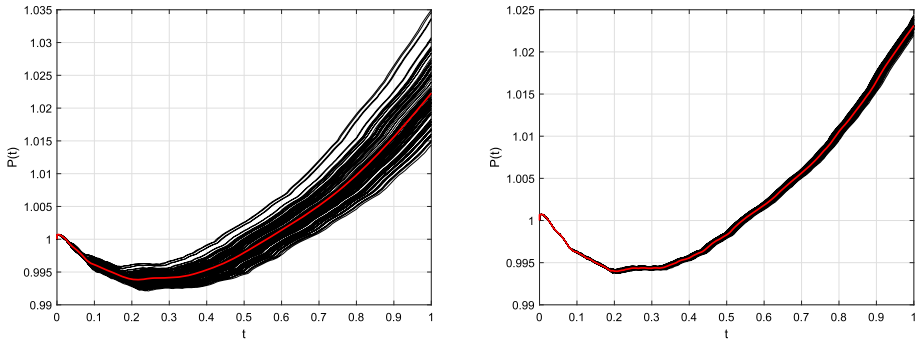

Fig. 9 Population samples for $K = 100$ in Example 5, where $D = 1$; left: $\eta_1(\omega) \sim \mathcal{B}e_{[1.6,\,2.4]}(2;\,4)$, right: $\eta_2(\omega) \sim \mathcal{B}e_{[1.6,\,2.4]}(200;\,400)$

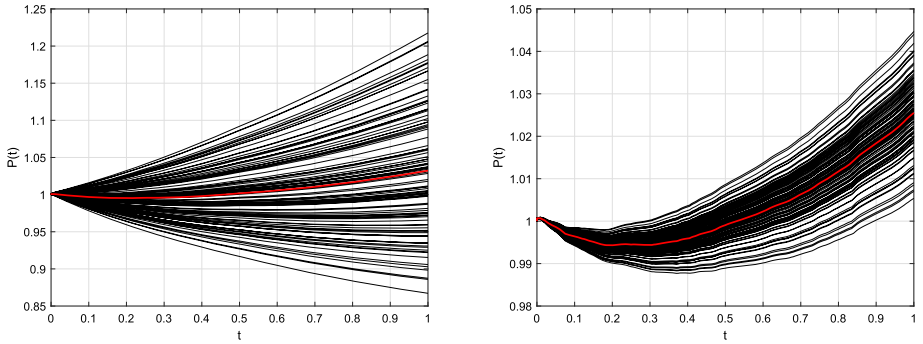

Fig. 10 Population samples for Example 5, where $\eta = 2$; left: $D_1(\omega) \sim \mathcal{N}_{[0.8,\,1.2]}(1,\,0.1)$, right: $D_2(\omega) \sim \mathcal{N}_{[0.8,\,1.2]}(1,\,0.01)$

7.3 Random case: spreading-vanishing dichotomy depending on the geometry of the habitat

In this subsection, we analyze how the spreading or vanishing behavior of the population depends not only on the parameters of the problem but also on the geometry of the initial habitat. We consider three main shapes of the habitat: an ellipse with a particular case of a circle, a rectangle with a particular case of a square, and an equilateral triangle.

Let us consider a RPDE (2)–(5) with $T = 5$, $\alpha = 1$, $\beta = 1$, and the random parameters $D(\omega) \sim \mathcal{N}_{[0.8,\,1.2]}(1,\,0.1)$, $\quad \eta(\omega) \sim \mathcal{B}e_{[1.6,\,2.4]}(2;\,4)$.

We perform $K = 100$ realizations of the Monte Carlo method on a domain $[-10,\,10] \times [-10,\,10]$ using a grid of 200×200 spatial nodes. As mentioned above, for underlying numerical scheme the RALADE method is employed.

For all cases, we fix the initial area and normalize the initial population density to ensure that at $t = 0$, it is equal to 1, as follows:

$$U_0(x, y) = \frac{u_0(x, y)}{P(0)}. \tag{91}$$

Example 6 Ellipse habitat: $\Phi_0 = \{(x, y) \in \mathbb{R}^2 : \frac{x^2}{a^2} + \frac{y^2}{b^2} \le 1\}$.

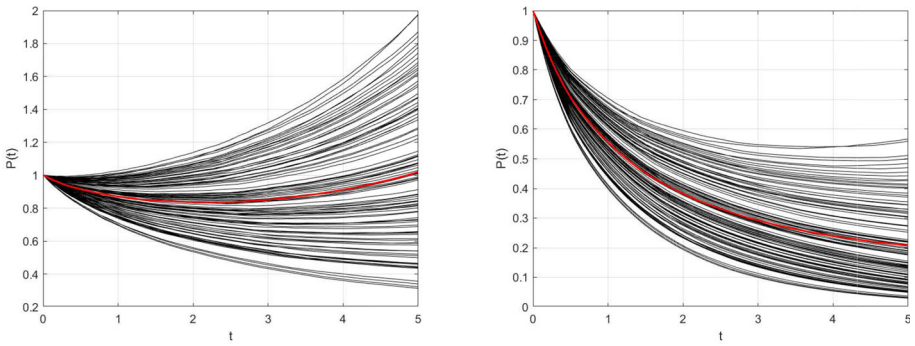

Fig. 11 Spreading-vanishing dichotomy of the population $P(t)$ in Example 6 for the habitat $\Phi_0 = \{(x, y) \in \mathbb{R}^2 : \frac{x^2}{a^2} + \frac{y^2}{b^2} \leq 1\}$ with the initial population density defined by (92). The red line represents the mean across all $K = 100$ realizations. Left plot shows the circular case with $a = b = 2.2$, while the right plot displays the ellipse case with $a = 3.67$ and $b = 1.32$

$$u_0(x, y) = 1 - \left(\frac{x^2}{a^2} + \frac{y^2}{b^2}\right). \tag{92}$$

We compare the propagation for various combinations of the parameters a and b with a normalized initial population density, specifically $P(0) = 1$. Let us introduce the parameter $r = 2.2$, which is the radius of the circle. Initially, we set $a = b = r$. In the deterministic case, with $D = 1$ and $\eta = 2$, we observe a scenario where vanishing behavior transforms into spreading, leading the population to recover the initial apparent vanishing values and subsequently continue growing. In the random case, we expect both spreading and vanishing due to the variability of the parameters. The population in each realization, in total $K = 100$ realizations, along with the corresponding mean depicted in solid line, is plotted in the left panel in Fig. 11.

Now, let us consider a general elliptic case. To maintain the initial area equal to that of the previously considered case ($\pi r^2 = \pi ab$), we keep $r = 2.2$. For a given value of b, we calculate $a = \frac{r^2}{b}$. For instance, we set $a = 3.67$ and $b = 1.32$. The population in each realization, along with the corresponding mean, is shown in the right plot of Fig. 11.

Observing the results plotted in Fig. 11, we notice that the initial circular habitat is more prone to spreading, whereas with the elliptical shape and the same initial population, vanishing is observed. Moreover, in the circular case, the mean population recovers the initial value (with further growth), whereas in the elliptical case, it steadily decreases. In other words, as eccentricity of the ellipse decreases the population behavior tends to be more prone to spreading.

Next, let us check how the initial population density distribution impacts the spreading. For that purpose, we consider the shifted function

$$u_0(x, y) = \sqrt{\left(y^2 - 2(b+1)y + 1 + (b+1)^2\right)\left(x^2 - 2(a+1)x + 1 + (a+1)^2\right)} \times \left(1 - \frac{x^2}{a^2} - \frac{y^2}{b^2}\right). \tag{93}$$

As in the previous case, we distinguish circular and elliptical initial habitats. The spreading-vanishing dichotomy remains similar to the previous case. Figures 12 and 13

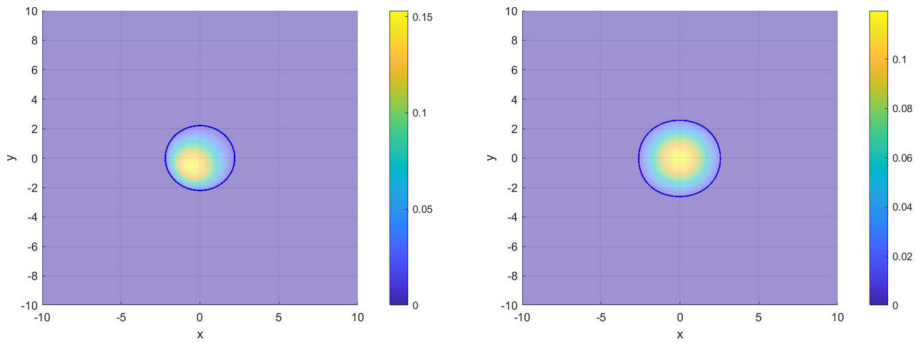

Fig. 12 Initial population distribution $u_0(x, y)$ defined by (93) (left plot) and the mean population distribution at $T = 5$ (right plot) for circular initial habitat shape in Example 6

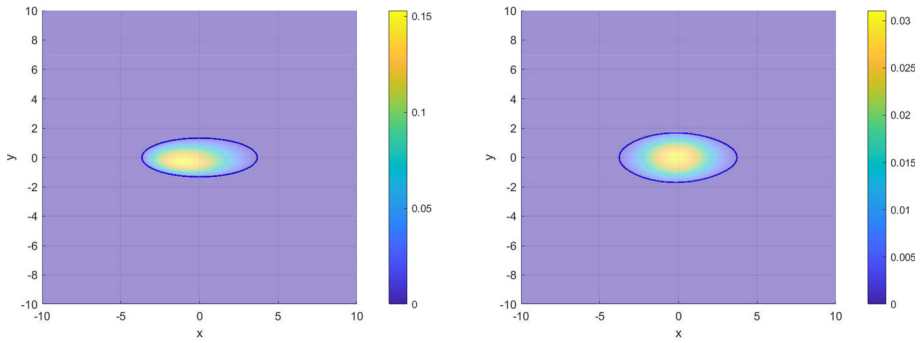

Fig. 13 Initial population distribution $u_0(x, y)$ defined by (93) (left plot) and mean population distribution at $T = 5$ (right plot) for elliptical initial habitat shape in Example 6

present the initial distribution and mean final distribution at $T = 5$ for the circular and elliptical forms, respectively. Upon observing the results, we note that the epicenter (core) tends to the center of the circle/ellipse. Furthermore, it is evident that elliptical forms tend to transform into circular forms over time.

Now, we examine the dynamics of populations within rectangular habitats, which provides a useful contrast to the more symmetric shapes studied earlier, offering insights into the effects of habitat shape on spreading capabilities.

Example 7 Rectangle habitat: $\Phi_0 = \{(x, y) \in \mathbb{R}^2 : |x| \le a, |y| \le b\}$.

Initial population distribution is given as follows

$$u_0(x, y) = (x^2 - a^2)(y^2 - b^2). \tag{94}$$

To maintain the same initial habitat area, for a fixed a, we set $b = \frac{\pi r^2}{4a}$, where r is the radius of the circular habitat in the previous example. Note that $a = \frac{r\sqrt{\pi}}{2}$ corresponds to the square habitat. In the case of $r = 2.2$, $a = b = 1.9497$. For the rectangular form, we set $a = 1.3648$ and $b = 2.7853$.

The front at the initial moment, and its mean at instants $T = 5$ and $T = 10$ for the square and rectangular habitat shapes are shown in Fig. 14. In both cases, the front tends to the circular form over time.

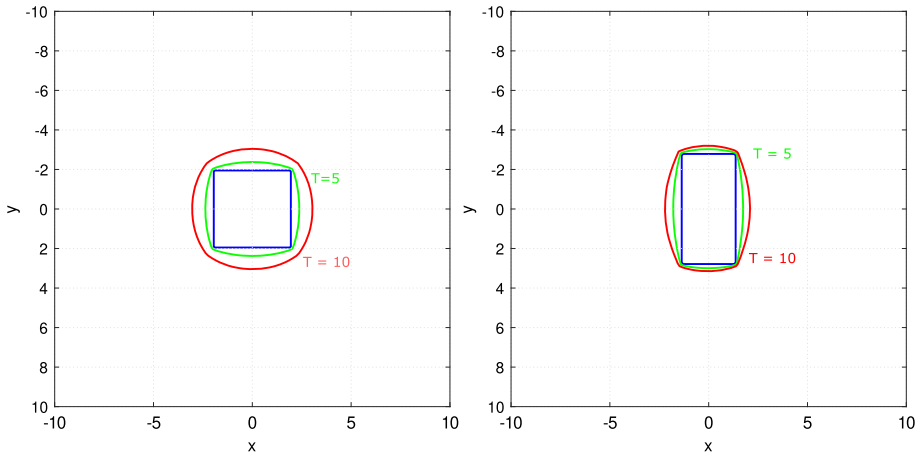

Fig. 14 Evolution of the mean of the population front at different times $T = \{0, 5, 10\}$ for the square (left plot) and rectangular (right plot) habitats in Example 7

Example 8 Equilateral triangle habitat: $\Phi_0 = \{(x, y) \in \mathbb{R}^2 :$ barycentric coordinates $\lambda_1, \lambda_2, \lambda_3$ satisfy $\lambda_1 + \lambda_2 + \lambda_3 = 1$ and $\lambda_1, \lambda_2, \lambda_3 \geq 0\}$, where $\lambda_1, \lambda_2, \lambda_3$ are the barycentric coordinates for the triangle defined as follows:

$$\lambda_1(x, y) = \frac{(y - y_2)(x_3 - x_2) - (x - x_2)(y_3 - y_2)}{(y_1 - y_2)(x_3 - x_2) - (x_1 - x_2)(y_3 - y_2)},$$
$$\lambda_2(x, y) = \frac{(y - y_3)(x_1 - x_3) - (x - x_3)(y_1 - y_3)}{(y_2 - y_3)(x_1 - x_3) - (x_2 - x_3)(y_2 - y_3)},$$
$$\lambda_3(x, y) = 1 - \lambda_1(x, y) - \lambda_2(x, y),$$

for the side length a, height $h = \frac{a\sqrt{3}}{2}$ and triangle vertex coordinates $v_1 = (x_1, y_1) = (-a/2, -h/3)$, $v_2 = (x_2, y_2) = (a/2, -h/3)$ and $v_3 = (x_3, y_3) = (0, 2h/3)$.

Following the ideas of Liu et al. (2020), we define the level set function as follows

$$\phi_0(x, y) = -\min(\lambda_1, \lambda_2, \lambda_3), \tag{95}$$

and the initial population distribution is given by

$$u_0(x, y) = \lambda_1 \cdot \lambda_2 \cdot \lambda_3. \tag{96}$$

To maintain the same initial habitat area as in previous examples, we set $a = r\sqrt{\frac{4\pi}{\sqrt{3}}}$, where r is the radius of the circular habitat. The evolution of the mean of the population front is presented in Fig. 16. As observed in previous examples, the habitat also tends to take on a circular shape. The population $P(t)$, depicted in Fig. 16 across $K = 100$ simulations of the Monte Carlo method, exhibits a spreading-vanishing dichotomy depending on the values of the r.v.'s $D(\omega)$ and $\eta(\omega)$.

To estimate the impact of initial habitat geometry on spreading, we analyze the previously described examples with different parameters in the following example.

Example 9 Evolution of the statistical moments of the approximations to the population density s.p. and the moving front s.p. attending to the initial habitat geometry.

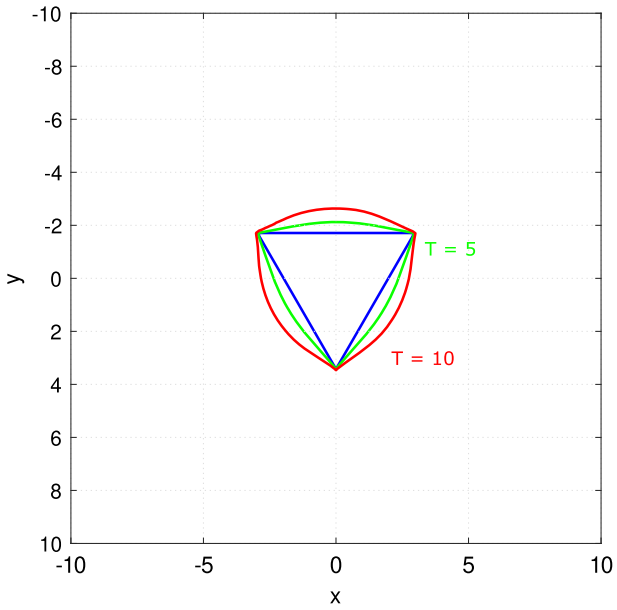

Fig. 15 Evolution of the mean of the population front at different times $T = \{0, 5, 10\}$ for the triangular habitat in Example 8

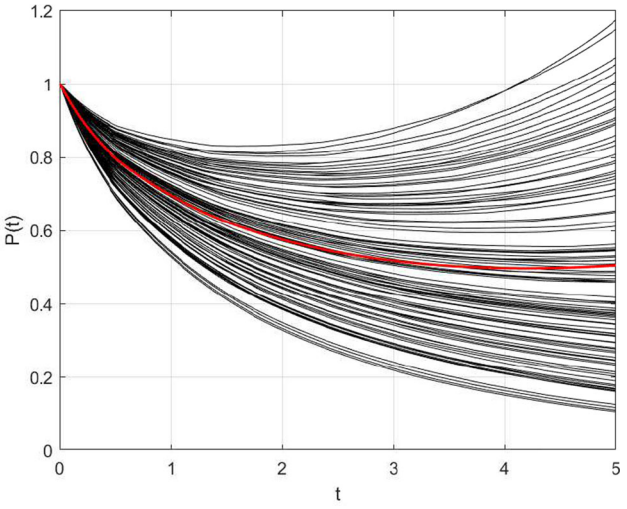

Fig. 16 Spreading-vanishing dichotomy of the population $P(t)$ in Example 8. The red line represents the mean across all $K = 100$ realizations

Table 3 collects the results of the comparison of various habitat geometries (column "Shape"). Specifically, we compare the mean population at the moment $T = 5$ (column "$\mu[P(T)]$"), considering that the initial population for all simulations is set to one. For each example, we calculate the percentage growth of the mean habitat area (column "Habitat Growth, %").

Table 3 Summary of simulation results ($K = 100$ samples of the Monte Carlo method) for different habitat shapes and normalized initial population $P(0) = 1$ at the moment $T = 5$

Shape	$\mu[P(T)]$	Habitat growth, %	Observations
Circle, $r = 2.2$	1.02	36.33	Vanishing-spreading
Circle, $r = 2.2$, shifted core	1.01	36.01	Vanishing-spreading
Ellipse, $b = 1.32$	0.2079	24.36	Vanishing
Ellipse, $b = 1.32$, shifted core	0.2090	24.36	Vanishing
Square, $a = 1.95$	0.8529	32.91	Vanishing-spreading
Rectangle, $a = 1.3648$, $b = 2.7853$	0.3795	27.25	Vanishing
Triangle, $a = 5.9258$	0.4513	29.56	Vanishing-spreading
Circle, $r = 2.4$	1.7290	35.56	Spreading
Ellipse, $b = 1.44$	0.3990	23.62	Vanishing
Square, $a = 2.13$	1.4851	32.68	Spreading
Rectangle, $a = 1.2762$, $b = 3.5449$	0.2731	22.29	Vanishing
Triangle, $a = 6.4645$	0.9196	29.31	Vanishing-spreading

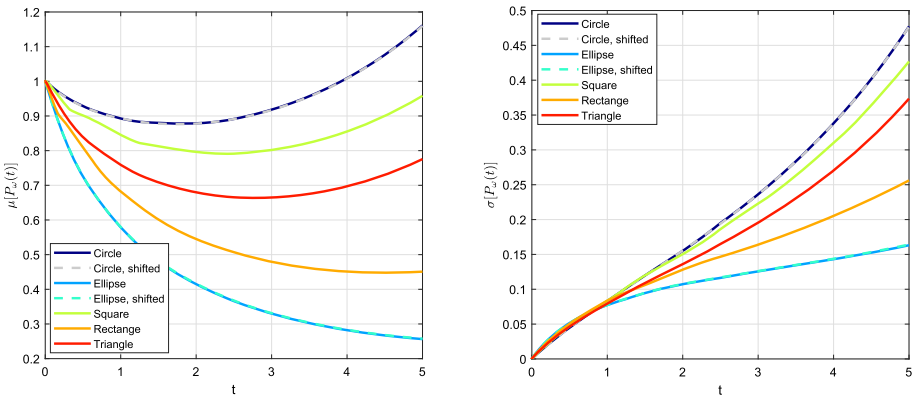

Fig. 17 Mean (left) and standard deviation (right) of the population $P(t)$ over time for various initial habitat shapes in Example 9 with $K = 100$ simulations

The simulations are divided into two groups. The first group corresponds to Examples 6, 7, and 8, where the initial habitat area is 15.2 square units for all cases. The second group of simulations has an initial habitat area of 18.1 square units, corresponding to the case of a circle with a radius $r = 2.4$. Hence, in each group, simulations are conducted with the same population distributed in habitats of different shapes but with equal areas. For each simulation case, we observe whether spreading or vanishing occurs (column "Observations"). It's important to note that if the population initially decreases and then starts to increase, we denote this situation vanishing-spreading behavior.

In Fig. 17, the mean and standard deviation of the population $P(t)$ are shown for the first group of the simulations. The standard deviation is higher when there are more opportunities for the population to spread. When the average population approaches zero, the standard deviation is smaller.

The comparison of results presented in Table 3 and Fig. 17 suggests that shapes with a more "rounded" profile exhibit a greater tendency for spreading when compared to more

"squashed" shapes. In the case of elliptical and rectangular shapes, there exists a critical ratio between the dimensions a and b that transitions vanishing behavior to spreading. A notable observation is that, even in instances of vanishing, the habitat area continues to increase, although at a slower rate. Across all considered cases, the habitat growth does not exceed 30% in the event of vanishing.

8 Conclusion

This study introduces a novel random numerical algorithm in the m.s. context to solve a random logistic free-boundary diffusion problems that integrates the RLSM and three explicit RFDS: REFDM, RIEFDM and RALADE. The extension from deterministic to the random framework is not so easy as it could be expected at a first glance due to storage accumulation task. Assuming sufficient conditions over both unknown stochastic processes: random front and random population density as well as over the random coefficients, we established conditions to formulate a well-posedness random system.

A key advantage of the RLSM lies in its ability to adapt to any habitat shape. This significantly enhances the versatility of our proposed algorithm. Unlike traditional models, the RLSM does not require the assumption of radial symmetry. This allows our approach to comprehensively investigate how the initial habitat's shape impacts the outcomes of spreading or vanishing phenomena. Our analysis revealed that habitats with more rounded and circular forms are inherently more prone to spreading. While habitats with flatter geometries show a greater resistance to spread, requiring more sources for expansion. The findings suggest that regardless of the initial shape, habitats tend to evolve towards a more circular geometry over time.

The numerical analysis of three proposed RFDS focuses on ensuring its m.s. stability, positivity, and boundedness. We established specific step size conditions that guarantee these properties, contributing to the algorithm's robustness. The m.s. consistency of the RFDS is studied in terms of the truncation error under hypotheses (6)–(7) and (10)–(11).

Numerical examples further validate these theoretical findings and provide an in-depth analysis of the numerical convergence of the interior solvers (RIEFDM and RALADE), alongside the convergence behavior of the Monte Carlo simulations. The use of the Monte Carlo method is a key piece to overcome the computational drawbacks related to the storage problems associated with computing of the expectation and variance of the approximate solution s.p. by the RLSM and RFDS developed above. Theoretical and numerical analyses reveal that RALADE emerges as the most favorable option among the considered RFDS due to its relaxed stability condition and better convergence properties.

In conclusion, this work introduces an efficient numerical algorithm for two-dimensional random logistic models with a free boundary, providing insights into the impact of habitat geometry on spreading and vanishing dynamics.

Acknowledgements This research is partially supported by the Spanish State Research Agency (AEI) through the project PDC2022- 400 133115-I00 entitled "B_2 F_2: Be a Better digital Fire-Fighter" funded by MCIN/AEI/10.13039/501100011033.

Author Contributions All authors contributed equally to this work. All authors read and approved the final manuscript.

Funding Open Access funding provided thanks to the CRUE-CSIC agreement with Springer Nature.

Data availability No datasets were generated or analysed during the current study.

References

Arif MS, Abodayeh K, Nawaz Y (2023) A reliable computational scheme for stochastic reaction-diffusion nonlinear chemical model. Axioms. https://doi.org/10.3390/axioms12050460

Aiki T, Muntean A (2013) A free-boundary problem for concrete carbonation: front nucleation and rigorous justification of the $\sqrt{t}$ -law of propagation. Interfaces Free Bound 15:167–180. https://doi.org/10.4171/IFB/299

Aronson DG, Weinberger HF (1978) Multidimensional nonlinear diffusion arising in population genetics. Adv Math 30:33–76. https://doi.org/10.1016/0001-8708(78)90130-5

Casabán MC, Company R, Egorova VN, Jódar L (2023) Qualitative numerical analysis of a free-boundary diffusive logistic model. Mathematics. https://doi.org/10.3390/math11061296

Casabán M-C, Company R, Egorova VN, Jódar L (2024) A random free-boundary diffusive logistic differential model: numerical analysis, computing and simulation. Math Comput Simul. https://doi.org/10.1016/j.matcom.2024.02.016

Casabán MC, Company R, Jódar L (2020) Numerical solutions of random mean square Fisher-KPP models with advection. Math Methods Appl Sci 43(14):8015–8031. https://doi.org/10.1002/mma.5942. https://onlinelibrary.wiley.com/doi/pdf/10.1002/mma.5942

Casabán MC, Company R, Jódar L (2021) Reliable efficient difference methods for random heterogeneous diffusion reaction models with a finite degree of randomness. Mathematics. https://doi.org/10.3390/math9030206

Cartwright M, Gottwald GA (2019) A collective coordinate framework to study the dynamics of travelling waves in stochastic partial differential equations. Physica D: Nonlinear Phenom 397:54–64. https://doi.org/10.1016/j.physd.2019.03.004

Du Y, Guo Z (2011) Spreading-vanishing dichotomy in a diffusive logistic model with a free boundary, II. J Differ Equ 250:4336–4366. https://doi.org/10.1016/j.jde.2011.02.011

Du Y, Lin Z (2010) Spreading-vanishing dichotomy in the diffusive logistic model with a free boundary. SIAM J Math Anal 42:377–405. https://doi.org/10.1137/090771089

Egorova VN, Tan SH, Lai CH, Company R, Jódar L (2017) Moving boundary transformation for American call options with transaction cost: finite difference methods and computing. Int J Comput Math 94:345–362. https://doi.org/10.1080/00207160.2015.1108409

Fisher RA (1937) The wave of advance of advantageous genes. Ann Eugenics 7:355–369

Gibou F, Fedkiw R, Osher S (2018) A review of level-set methods and some recent applications. J Comput Phys 353:82–109. https://doi.org/10.1016/j.jcp.2017.10.006

Kloeden P, Han X (2017) Random ordinary differential equations and their numerical solution. Springer, New York

Khan K, Liu S, Schaerf TM, Du Y (2021) Invasive behaviour under competition via a free boundary model: a numerical approach. J Math Biol. https://doi.org/10.1007/s00285-021-01641-y

Kolmogorov A, Petrovsky N, Piscounov S (1937) Étude de l'équations de la diffusion avec croissance de la quantité de matière et son application a un problème biologique. Bull Univ Moskou 1:1–25

Kröner D (1997) Numerical schemes for conservation laws. Wiley and Teubner, Hoboken

Larkin BK (1964) Some stable explicit difference approximations to the diffusion equation. Math Comput 18(86):196–202

Liu S, Du Y, Liu X (2020) Numerical studies of a class of reaction–diffusion equations with Stefan conditions. Int J Comput Math 97:959–979. https://doi.org/10.1080/00207160.2019.1599868

Liu S, Liu X (2024) Exponential time differencing method for a reaction–diffusion system with free boundary. Commun Appl Math Comput 6:354–371. https://doi.org/10.1007/s42967-023-00261-1

Malchow H (2008) Spatiotemporal patterns in ecology and epidemiology. Chapman and Hall/CRC, New York. https://doi.org/10.1201/9781482286137

Méndez V, Llopis I, Campos D, Horsthemke W (2011) Effect of environmental fluctuations on invasion fronts. J Theor Biol 281:31–38. https://doi.org/10.1016/j.jtbi.2011.04.025
Mentrelli A, Pagnini G (2016) Modelling and simulation of wildland fire in the framework of the level set method. Ricerche di Matematica 65:523–533. https://doi.org/10.1007/s11587-016-0272-1
Mitchell SL, Vynnycky M (2016) On the accurate numerical solution of a two-phase Stefan problem with phase formation and depletion. J Comput Appl Math 300:259–274. https://doi.org/10.1016/j.cam.2015.12.021
Nandi S, Sanyasiraju YVSS (2022) A second order accurate fixed-grid method for multi-dimensional Stefan problem with moving phase change materials. Appl Math Comput. https://doi.org/10.1016/j.amc.2021.126719
Nepal S, Ögren M, Wondmagegne Y, Muntean A (2023) Random walks and moving boundaries: estimating the penetration of diffusants into dense rubbers. Probab Eng Mech. https://doi.org/10.1016/j.probengmech.2023.103546
Osher S, Fedkiw RP (2001) Level set methods: an overview and some recent results. J Comput Phys 169:463–502. https://doi.org/10.1006/JCPH.2000.6636
Osher S, Fedkiw R (2003) Level set methods and dynamic implicit surfaces. Springer, New York
Osher S, Sethian JA (1988) Fronts propagating with curvature-dependent speed: algorithms based on Hamilton–Jacobi formulations. J Comput Phys 79:12–49. https://doi.org/10.1016/0021-9991(88)90002-2
Piqueras MA, Company R, Jódar L (2017) A front-fixing numerical method for a free boundary nonlinear diffusion logistic population model. J Comput Appl Math 309:473–481. https://doi.org/10.1016/j.cam.2016.02.029
Plemmons RJ (1977) M-matrix characterizations. I-Nonsingular M-matrices. Linear Algebra Appl 18:175–188. https://doi.org/10.1016/0024-3795(77)90073-8
Sethian JA (1996) A fast marching level set method for monotonically advancing fronts. Proc Natl Acad Sci USA 93:1591–1595
Shigesada N, Kawasaki K (1997) Biological invasions: theory and practice. Oxford University Press, Oxford
Singla T, Kumar B, Sharma S (2024) Numerical study of the melting process of spherical phase change material with variable thermal conductivity. Indian J Phys 98:1355–1363. https://doi.org/10.1007/s12648-023-02886-7
Smith GD (1985) Numerical solution of partial differential equations: finite difference methods, 3rd edn. Clarendon Press, Oxford
Soong TT (1973) Random differential equations in science and engineering. Academic Press, New York
Villafuerte L, Braumann CA, Cortés JC, Jódar L (2010) Random differential operational calculus: theory and applications. Comput Math Appl 59:115–125. https://doi.org/10.1016/j.camwa.2009.08.061
Wei P, Wang W, Yang Y, Wang MY (2020) Level set band method: a combination of density-based and level set methods for the topology optimization of continuums. Front Mech Eng 15:390–405. https://doi.org/10.1007/s11465-020-0588-0